NASA-CR-194,472

NASA
Contractor Report 194472

Army Research Laboratory
Contractor Report ARL–CR–72

# A Procedure for 3-D Contact Stress Analysis of Spiral Bevel Gears

NASA-CR-194472
19940028423

A. Kumar
*University of Akron*
*Akron, Ohio*

and

G. Bibel
*University of North Dakota*
*Grand Forks, North Dakota*

March 1994

LIBRARY COPY
JUN 23 1994
LANGLEY RESEARCH CENTER
LIBRARY, NASA
HAMPTON, VIRGINIA

Prepared for
Lewis Research Center
Under Contract NAG3–1476

National Aeronautics and
Space Administration

U.S. ARMY
RESEARCH LABORATORY

NASA Technical Library
3 1176 01408 8174

# A PROCEDURE FOR 3-D CONTACT STRESS ANALYSIS

# OF

# SPIRAL BEVEL GEARS

A. Kumar
University of Akron
Akron, Ohio

G. Bibel
University of North Dakota
Grand Forks, North Dakota

**ABSTRACT**

Contact stress distribution of spiral bevel gears using non-linear finite element static analysis is presented. Procedures have been developed to solve the non-linear equations that identify the gear and pinion surface coordinates based on the kinematics of the cutting process; and, orientate the pinion and the gear in space to mesh with each other. Contact is simulated by connecting GAP elements along the intersection of a line from each pinion point (parallel to the normal at the contact point) with the gear surface. A three - dimensional model with four gear teeth and three pinion teeth is used to determine the contact stresses at two different contact positions in a spiral bevel gearset. A summary of the elliptical contact stress distribution is given. This information will be helpful to helicopter and aircraft transmission designers who need to minimize weight of the transmission and maximize reliability.

## TABLE OF CONTENTS


| | PAGE |
|---|---|
| ABSTRACT | i |
| LIST OF FIGURES | iv |
| LIST OF TABLES | vii |
| CHAPTER | |
| I. INTRODUCTION | 1 |
| II. GEAR SURFACE GEOMETRY | 3 |
| 2.1 GEAR MANUFACTURE | 3 |
| 2.2 TOOTH SURFACE COORDINATE SOLUTION PROCEDURE | 5 |
| 2.3 COORDINATE TRANSFORMATIONS | 8 |
| 2.4 APPLICATION OF SOLUTION TECHNIQUE | 13 |
| 2.5 CONCAVE AND CONVEX ORIENTATIONS | 16 |
| 2.6 GEAR AND PINION ORIENTATIONS | 16 |
| III. CONTACT SIMULATION WITH GAP ELEMENTS | 18 |
| 3.1 PROCEDURE TO FIND THE CONTACT POINT | 18 |
| 3.2 PROCEDURE TO DETERMINE THE NORMAL VECTOR | 19 |
| 3.3 PROCEDURE TO DETERMINE THE INTERSECTION OF NORMAL VECTOR WITH GEAR SURFACE | 23 |
| 3.4 VERIFICATION OF THE INTERSECTION POINT | 27 |
| IV. NUMERICAL EXAMPLES | 29 |
| 4.1 MODEL DESCRIPTIONS | 29 |
| V. DISCUSSIONS OF RESULTS | 33 |

VI. CONCLUSIONS ..... 36

VII. REFERENCES ..... 37

LIST OF FIGURES Page


Figure 1 Machine used to generate spiral bevel gear surface..... 38

Figure 2 Machining process with workpiece and cutter orientations ..... 39

Figure 3 Projection of gear tooth surface into XZ plane ..... 40

Figure 4 Right and left hand spiral bevel gears .. 41

Figure 5 Orientation of coordinate system for cutter, cradle and system fixed to machine frame . 42

Figure 6 Machine settings and orientation with rotation of workpiece during tooth surface generation ..... 43

Figure 7 Convex and concave orientations to obtain desired top land ..... 44

Figure 8 Gear and pinion orientations required for meshing..... 45

Figure 9 Different sections taken along the pinion spiral ..... 46

Figure 10 Cutting head cone surface normal ..... 47

Figure 11 Rotations required to solve for intersection of pinion normal with gear surface normals ..... 48

Figure 12 Illustration to show intersecting normal with the gear convex surface ..... 49

Figure 13 Gear geometry distortion after connecting gap elements ..... 50

Figure 14 Model I: Pinion and gear tooth in mesh with boundary conditions ..... 51

Figure 15 Model I: Minimum principal element stresses in pinion tooth ..... 52

Figure 16 Model I: Minimum principal element stresses in pinion ..... 53

Figure 17 Model I: Average nodal minimum principal stresses in pinion tooth ..... 54

Figure 18 Model I: Average nodal minimum principal stresses in pinion at contact region..... 55

Figure 19 Model I: Gap element status at each iteration ..... 56

Figure 20 Model II: Mesh generation with boundary conditions ..... 57

Figure 21 Model II: Minimuml principal element stresses at major contact region of pinion tooth ..... 58

Figure 22 Model II: Minimum principal element stresses at major contact region in pinion ..... 59

Figure 23 Model II: Average nodal minimum principal stresses in pinion having major contact . 60

Figure 24 Model II: Average nodal minimum principal stresses in pinion at major contact region ..... 61

Figure 25 Model II: Minimum principal element stresses in pinion tooth having edg2 contact ..... 62

Figure 26 Model II: Minimum principal element stresses at edge contact region in pinion ..... 63

Figure 27 Model II: Average nodal minimum principal stresses in pinion having edge contact .. 64

Figure 28 Model II: Average nodal minimum principal stresses in pinion at edge contact region ..... 65

Figure 29 Model II: Gap element status at each iteration ..... 66

Figure 30 Model III: Finite element mesh and boundary conditions ..... 67

Figure 31 Model III: Minimum principal element stresses in pinion at major contact region ...68

Figure 32 Model III: Nodal minimum principal stresses in pinion at major contact region ...69

Figure 33 Model III: Element principal stresses in pinion having edge contact..... 70

Figure 34 Model III: Nodal principal stresses in pinion having edge contact..... 71

Figure 35 Model III: Gap element status at each iteration ..... 72

Figure 36 Approximate Contact region ..... 73

Figure 37 Contact area calculation ..... 74

**LIST OF TABLES** **Page**

Table I. MODEL - 1: Minimum Principal Stress results ..... 74

Table II. MODEL - 2: Minimum Principal Stress results ..... 75

Table III. MODEL - 3: Minimum Principal Stress results ..... 76

# CHAPTER I

# INTRODUCTION

Spiral bevel gears are used to transmit power between intersecting shafts. One critical application is a helicopter transmission in which power is transmitted from the horizontal engine to the vertical rotor shaft.

These gears operate at relatively high rotational speeds and transmit substantial power. (i. e. 15,000 rpm and 900 hp) Accurate prediction of tooth bending and contact stresses are important to design stronger, lighter gears with longer service lives.

Much effort has focused on predicting stresses in gears with the finite element method. Most of this work has involved parallel axis gears with two dimensional models. Parallel axis components have closed form solutions that determine surface coordinates. Spiral bevel gears, however, do not have closed form solutions available to identify surface coordinates.

Only a few researchers have investigated finite element analysis of spiral bevel gears. [1-3] The research reported here will develop a finite element model to study meshing of a spiral bevel gearset. Pinion and gear tooth surfaces will be developed based on the kinematics of gear

manufacture. The individual teeth are then rotated in space to create a multi-tooth model.

The initial model has one pinion tooth and one gear tooth. Subsequent models consist of four gear teeth and three pinion teeth. The tooth pair contact zones are modeled with GAP elements. The model development procedures and finite element results are presented.

# CHAPTER II

# GEAR SURFACE GEOMETRY

This chapter describes the gear manufacturing process, the kinematics of cutting, tooth surface coordinate solution procedure, concave and convex surface rotations of the gear and pinion, and different orientations required for the spiral bevel gears to mesh with each other. Also described is the transformation process which transforms a point on the cutting blade to a point on the workpiece. Application of tooth surface coordinate solution technique is also described.

## 2.1 GEAR MANUFACTURE

The Gleason Works, Rochester, NY, provides machinery for the manufacture of spiral bevel gears. The machine shown in figure (1) is used to cut these gears [4]. These machines are preferred because they can be used for both milling and grinding operations. Grinding is especially important for producing hardened high quality aircraft gears. This machine consists of three main parts: the machine frame, the cradle and the sliding base. The gear cutter is mounted to the cradle of the cutting machine. The machine cradle with the cutter may be imagined as a crown gear that meshes with the gear being cut as shown in figure (2). The gear which is being cut and the cradle with the mounted head cutter rotates

slowly about its own axis. The combined process generates the gear tooth surface.

The cradle rotates far enough so that only one space between the tooth is cut out. It then reverses rapidly while the workpiece is withdrawn from the cutter and indexed ahead by the translation of the sliding base (on which the work is mounted) with respect to the cutter, in preparation for the next tooth. This sequence of operations is repeated till the last tooth is cut [4].

The head cutter, which holds the cutting blades or the grinding wheels, is shown in figure (2). The cutter carries blades of straight lined-profile which generate a cone during rotation. It rotates about its own axis C-C at a speed for efficient metal removal, independent of the cradle or workpiece rotations. The head cutter is connected to the cradle through an eccentric that allows adjustment of the axial distance between the cutter center and the machine center. The adjustment of the angular position between the two axes provides the desired spiral angle.

The pinion is typically cut on one side at a time, concave and convex tooth sides, whereas the gear is cut both sides simultaneously (duplex method). The cradle and workpiece are

connected through a system of gears and shafts, which controls the ratio of rotational motion between the two. This ratio is called the ratio of roll. For cutting, the ratio is constant; but for grinding it is a variable.

## 2.2 TOOTH SURFACE COORDINATE SOLUTION PROCEDURE

From the kinematics of the manufacturing process an analytical method was developed by Litvin [4,5] to generate the surface coordinates of spiral bevel gears. The manufacturing data, the surface geometry and the equation of meshing are used to develop the equations.

The first equation is the EQUATION OF MESHING given in reference [4-6]. This equation is based on the kinematics of manufacture and the machine tool settings. The equation of meshing requires that the relative velocity between a point on the cutting surface and the same point on the pinion being cut must be perpendicular to the cutting surface normal.

This is given by:

$$\mathbf{n} \cdot \mathbf{V} = 0$$

where '**n**' is the normal vector to the cutter and the workpiece surfaces at the specified location of interest, and '**V**' is the relative velocity between the cutter and the

workpiece surfaces at the specified location. This equation is developed in terms of the machine tool coordinates $u, \theta, \phi_c$ where $u$ and $\theta$ (length and rotational orientation) locate a point on the cutting head cone and $\phi_c$ is the rotated orientation of the cutter as it swings on the cradle. This equation which is in terms of $(u, \theta, \phi_c)$ could be transformed into $(x, y, z)$ coordinate system using the transformation process described in the next section. The equation of meshing for straight sided cutters with a constant ratio of roll and left-hand spiral tooth is given by [4-6]

$$
\begin{aligned}
&(u - r\cot\psi \cos\psi)\cos\gamma \sin\tau \\
&+ s[(m_{cw} - \sin\gamma)\cos\psi \sin\theta \\
&- \cos\gamma \sin\psi \sin(q - \phi_c)] \\
&+ E_m(\cos\gamma \sin\psi + \sin\gamma \cos\psi \cos\tau) \\
&- L_m \sin\gamma \cos\psi \sin\tau = 0
\end{aligned}
\qquad (2.2.1)
$$

Where $\gamma$ is the root angle of the gear being manufactured, $\psi$ the blade angle, $q$ the cradle angle and $\tau$ equals $(\theta - q + \phi_c)$.

Since the equation of meshing has three unknown parameters $u$, $\theta$, $\phi_c$, two more equations have to be developed to solve for points on the surfaces. The two other equations are obtained considering the pinion and gear geometry.

The orientation of the gear on a coordinate system with the apex of the cone at the origin is as shown in figure (3).

Any point on this surface is located by determining **'r'** and **'z'** coordinates when projected on to the **XY** plane. These are determined using the geometry of the gear.

The value of $Z_w$, found by the transformation process of a point from the head cutter to the workpiece surface, should match the value of $Z_{bar}$ found by the projection of the tooth in the **XY** plane. To satisfy this condition the following equation is used. [1]

$$Z - Z_{bar} = 0 \quad \text{.....( 2.2.2)}$$

The radial location of a point from the work axis of rotation must be equal to the value of r as shown in figure 3. This forms the third equation [1]

$$R_{bar} - \sqrt{(x_w^2 + y_w^2)} \quad \text{.....( 2.2.3)}$$

These three above equations could be written as

$$f_1(u, \theta, \phi_c) = 0$$
$$f_2(u, \theta, \phi_c) = 0$$
$$f_3(u, \theta, \phi_c) = 0 \quad \text{.....(2.2.4)}$$

## 2.3 COORDINATE TRANSFORMATIONS

The purpose of the coordinate transformations are to transform a point on the cutting head to a point on the

workpiece. These points on the workpiece will then describe the gear surface geometry. During the cutting process, the cutting head acts as if in mesh with a simulated crown gear. Therefore, the appropriate point in the cutting head is a point that satisfies the equation of meshing. (i. e. the normal of the point on the generating surface should be perpendicular to the relative velocity between the cutter and the gear tooth surface.)

To perform these transformations homogeneous coordinates are used to allow rotations and translations of vectors by simply multiplying the matrix transformations. To transform a point on the cutting head to the workpiece five such transformations are carried out. These are as follows [4-6]:

1. Cutter coordinates ($S_c$) --> Cradle coordinates ($S_s$)
2. Cradle coordinates ($S_s$) --> Machine fixed ($S_m$)
3. Machine fixed ($S_m$) --> Pinion-pitch angle ($S_p$)
4. Pinion-pitch angle ($S_p$) --> Pinion axis of rotation ($S_a$)
5. Pinion axis of rotation ($S_a$) --> Pinion fixed system ($S_w$)

Before discussing these the following points should be noted:

1. The head cutter coordinate system $S_c$ is rigidly connected to the coordinate system $S_s$. The system $S_s$ is rigidly

connected to the cradle that rotates about the $\mathbf{X_m}$ axis of the machine coordinate system $\mathbf{S_m}$.

2. The cutting head is attached to the cradle with a specific orientation '**s**' and '**q**' where '**s**' is the distance between $\mathbf{S_s}$ and $\mathbf{S_c}$ origins ($\mathbf{s} = O_cO_s$) and $\phi_c$ is the roll angle of the cradle.

3. The cradle rotates at a constant $\omega$ ($\omega_{cradle}$ or $\omega_c$).

4. The workpiece rotates at a constant $\omega$ ($\omega_{workpiece}$ or $\omega_w$).

5. The ratio of $\omega_{cradle}/\ \omega_{workpiece}$ is the same as the ratio of angular velocity of the simulated crown gear meshing with the gear being cut.

6. The cutting head rotation is not relevant. It only effects the metal removal rates. It is helpful to think of the cutting head as being fixed. The cradle rotation sweeps the cutting head cone through the workpiece cone. The interference between the two shapes the tooth surface.

7. The orientations of the coordinate transformations are different for left-hand and right-hand gears. The Gear tooth spirals to the left while looking from the front of the gear (the front is being viewed from the apex) in case of left-hand gear whereas, for the right-hand gear it spirals to the right (see figure 4). In the following discussions the left-hand gear transformations are described exclusively.

Beginning with a point on the cutting blade given by [4-6]:

$$\bar{r}_c = \begin{bmatrix} r\cos\psi - u\cos\psi_c \\ u\sin\psi_c\sin\theta \\ u\sin\psi_c\cos\theta \\ 1 \end{bmatrix} \qquad (2.3.1)$$

where '**r**' is the radius of the blade at $x_c$=0 in figure (2), and '$\psi$' is the blade angle. Parameters **u** and $\theta$ locate a point in the system $S_c$ and are unknowns, whose values will be determined.

To transform the head cutter into coordinate system $S_s$, the following matrix is used :

$$[M_{sc}] = \begin{bmatrix} 1 & 0 & 0 & 0 \\ 0 & \cos q & -\sin q & -s\sin q \\ 0 & \sin q & \cos q & s\cos q \\ 0 & 0 & 0 & 1 \end{bmatrix} \qquad (2.3.2)$$

where '**q**' is the cradle angle and '**s**' is the distance between the coordinate systems $S_s$ and $S_c$ as shown in figure 5. In this view, $X_m$ the axis of rotation of the cradle, and $X_c$ the axis of rotation of the cutting head are coming out of the page. These are parallel to each other and fixed in space. '**s**' and '**q**' are polar coordinates in the $S_s$ coordinate system that locate the cutting head. They are different for each gear design. Once the cutting head is located on the cradle for a specific design, it is locked in place with '**s**' and '**q**' being fixed and constant for the manufacture of that gear. [Msc]* $\bar{r}_c$ is the coordinate of a point in the $S_s$ coordinate system.

To transform $S_s$ to the fixed coordinate system $S_m$ the following transformation is used:

$$M_{ms} = \begin{bmatrix} 1 & 0 & 0 & 0 \\ 0 & \cos\phi_c & \sin\phi_c & 0 \\ 0 & -\sin\phi_c & \cos\phi_c & 0 \\ 0 & 0 & 0 & 1 \end{bmatrix} \tag{2.3.3}$$

where $\phi_c$ is the roll angle of the cradle. The coordinate system $S_m$ is fixed in space. The origin of $S_m$ is at the center of rotation of the cradle. The origins $O_m$ and $O_s$ coincide as shown in the figure (5). The rotation of $S_s$ relative to $S_m$ indicates how much the cradle has rotated. [Mms] [Msc] * $\bar{r}_c$ are the coordinates of a point in the coordinate system $S_m$.

The third coordinate transformation is from the coordinate system $S_m$ to $S_p$ which orients the pitch apex of the gear being manufactured. This transformation requires special machine tool settings $L_m$ and $E_m$ along with the dedendum angle which is obtained from the design data. The values of $L_m$ and $E_m$ settings could be obtained from table I. The coordinate system orientation to generate a left hand gear surface is shown in figure (5).

The transformation matrix is given by:

$$M_{pm} = \begin{bmatrix} \cos\delta & 0 & -\sin\delta & -L_m \sin\delta \\ 0 & 1 & 0 & +E_m \\ \sin\delta & 0 & \cos\delta & L_m \cos\delta \\ 0 & 0 & 0 & 1 \end{bmatrix} \tag{2.3.4}$$

The next transformation rotates a point from $S_p$ to $S_a$. This is well illustrated in figure 6. The common origin of $S_p$ and $S_a$ locates the apex of the gear under consideration with respect to the $S_m$ coordinate system. This requires a rotation about $Y_a$ by the pitch angle $\mu$. This is given by the matrix shown below:

$$M_{ap} = \begin{bmatrix} \cos\mu & 0 & -\sin\mu & 0 \\ 0 & 1 & 0 & 0 \\ -\sin\mu & 0 & \cos\mu & 0 \\ 0 & 0 & 0 & 1 \end{bmatrix} \tag{2.3.5}$$

The final transformation is from the coordinate system $S_a$ to coordinate system $S_w$, which is fixed to the component being manufactured. A rotation about the $Z_p$ axis is required through an angle $\phi_w$, as shown in figure 6. This transformation is given by:

$$M_{wa} = \begin{bmatrix} \cos\phi_w & \sin\phi_w & 0 & 0 \\ -\sin\phi_w & \cos\phi_w & 0 & 0 \\ 0 & 0 & 1 & 0 \\ 0 & 0 & 0 & 1 \end{bmatrix} \tag{2.3.6}$$

Using these five transformations any point in the head cutter coordinate system can be transformed into the workpiece coordinate system with this equation [4-6] :

$$\bar{r}_w = [M_{wa}]\ [M_{ap}]\ [M_{pm}]\ [M_{ms}]\ [M_{sc}] \begin{bmatrix} r\cos\psi - u\cos\psi_c \\ u\sin\psi_c \sin\theta \\ u\sin\psi_c \cos\theta \\ 1 \end{bmatrix} \qquad (2.3.7)$$

## 2.4 APPLICATION OF SOLUTION TECHNIQUE

The three equations discussed earlier to describe the surface coordinates are non-linear equations which do not have a closed form solution. These are solved using a numerical technique. These three equations could be rewritten as

$$\bar{F}\ (u,\ \theta,\ \phi_C) = \begin{bmatrix} f_1(u,\ \theta,\ \phi_C) = 0 \\ f_2(u,\ \theta,\ \phi_C) = 0 \\ f_3(u,\ \theta,\ \phi_C) = 0 \end{bmatrix} \qquad (2.4.1)$$

or

$$\bar{F}(\bar{x}) = 0 \qquad (2.4.2)$$

where

$$\bar{X} = \begin{bmatrix} u \\ \theta \\ \phi_C \end{bmatrix} \qquad (2.4.3)$$

The equation of meshing which is written in terms of ( $u$, $\theta$, $\phi_c$ ), is numerically differentiated by adding small increments using a five point formula [7], and then

coordinate transformations are used to convert the change in **u**, $\theta$, $\phi_c$ into change in x,y,z. By doing so the values of

$$\frac{\partial f_1}{\partial x_1}, \frac{\partial f_1}{\partial x_2}, \frac{\partial f_1}{\partial x_3}$$

are calculated. The other two equations are already in the **x,y,z** coordinates. Newtons method [7] is then used to solve the equations . The procedure is as follows:

Starting with an initial guess $X^\circ$ for the three parameters $X_1$, $X_2$ and $X_3$ , $\bar{F}(\bar{x}^\circ)$ is calculated. From this we obtain

$$\bar{F}(\bar{x}^\circ) = \begin{bmatrix} f_1(X^\circ) \\ f_2(X^\circ) \\ f_3(X^\circ) \end{bmatrix} \tag{2.4.4}$$

Now, calculating the Jacobian for $X^\circ$, nine specific values are obtained.

$$\begin{bmatrix} \frac{\partial f_1(X^\circ)}{\partial x_1} & \frac{\partial f_1(X^\circ)}{\partial x_2} & \frac{\partial f_1(X^\circ)}{\partial x_3} \\ \frac{\partial f_2(X^\circ)}{\partial x_1} & \frac{\partial f_2(X^\circ)}{\partial x_2} & \frac{\partial f_2(X^\circ)}{\partial x_2} \\ \frac{\partial f_3(X^\circ)}{\partial x_1} & \frac{\partial f_3(X^\circ)}{\partial x_2} & \frac{\partial f_3(X^\circ)}{\partial x_3} \end{bmatrix} \tag{2.4.5}$$

This Jacobian is formed by numerical differentiation and evaluating the derivatives at the initial guess.

The set of non-linear equations can now be transformed into a set of linear equations. This is done as follows:

$$\begin{bmatrix} \frac{\partial f_1(X^\circ)}{\partial X_1} & \frac{\partial f_1(X^\circ)}{\partial X_2} & \frac{\partial f_1(X^\circ)}{\partial X_3} \\ \frac{\partial f_2(X^\circ)}{\partial X_1} & \frac{\partial f_2(X^\circ)}{\partial X_2} & \frac{\partial f_2(X^\circ)}{\partial X_3} \\ \frac{\partial f_3(X^\circ)}{\partial X_1} & \frac{\partial f_3(X^\circ)}{\partial X_2} & \frac{\partial f_3(X^\circ)}{\partial X_3} \end{bmatrix} * \begin{bmatrix} Y_1 \\ Y_2 \\ Y_3 \end{bmatrix} = \begin{bmatrix} f_1(X^\circ) \\ f_2(X^\circ) \\ f_3(X^\circ) \end{bmatrix}$$

The solution to this set of linear equations is used as the guess to obtain the solution in the next iteration. This process is repeated until the difference between the solutions in two consecutive iterations is within the required tolerance.

$$X^1 = X^o + Y$$

or;

$$U^1 = U^o + Y_1$$

$$\theta^1 = \theta^o + Y_2$$

$$\phi_c{}^1 = \phi_c{}^o + Y_3$$

The variables used to define the above parameters are given in reference [3] which illustrates the numerical example solved for a specific design data.

## 2.5 CONCAVE AND CONVEX ORIENTATIONS

The orientations are performed in order to obtain the top land on the gear and pinion tooth. The top land thickness is calculated at the face angle on the toe end of the gear tooth. In figure 7, P1 is the concave side location of the face angle point at the toe end of the tooth,

P2 and P2' are the initial and final convex locations of the face angle point at the toe end of the tooth [3]. These points are described in coordinate system $S_w$. $T_a$ and $T_b$ are the desired and initial top land thickness for the gear tooth. By rotating the convex side points of the gear tooth by an angle $\varepsilon$ the desired thickness for the gear tooth is obtained.

## 2.6 GEAR AND PINION ORIENTATIONS

The apex of the pinion and the gear cones generated meet at a point as shown in figure 8. To place the gear and pinion in mesh with each other the following rotations are carried out.

(i) The pinion is rotated about its own axis by a very small rotation angle in the counter clockwise direction about the Z axis. The amount of rotation is determined by observing contact with the three dimensional geometric modeling program (TDGMP) [8]. The amount of rotation used for the example presented in Chapter V is 3.56 degrees.

(ii) The second transformation is the rotation of all the surface points obtained from the previous transformation about the global Y axis by 90 degrees in the counter

clockwise direction. This transformation places the pinion over the gear as shown in figure 8.

(iii) The third transformation is to rotate the gear tooth surface points by $(360/N_t) + 180$ degrees about the global Z axis in the clockwise direction. By doing so the gear tooth generated, meshes with the pinion as shown. The rotation used in this study was 190 degrees.

# CHAPTER III

# CONTACT SIMULATION WITH GAP ELEMENTS

After the gear and the pinion are oriented in mesh with each other, the contact is simulated by connecting GAP elements. An assumed contact point is found on the pinion concave surface and then the normal vector is calculated from this point. The intersection of the normal vector with the gear convex surface is found. The intersection of parallel vectors from neighboring grid points are also found. These points are connected to form the GAP elements. The solution technique which performs these steps is presented in this chapter.

## 3.1 PROCEDURE TO FIND THE CONTACT POINT

After orienting the pinion concave surface to be in mesh with the gear convex surface, the two surfaces are viewed in TDGMP [8] to find an approximate area of contact. This is done at various slices across the section of the gear surfaces in the direction of the spiral angle as shown in the figure 9. Having found the area of contact, the two closest grid points are chosen to be the contact point.

## 3.2 PROCEDURE TO DETERMINE THE NORMAL VECTOR

The equations used to find out the normal vector is provided by Litvin [4]. The normal vector is first found in

the head-cutter coordinate system and then is transformed to the workpiece coordinate system using the transformations described in chapter II.

Any point in the tool surface which is a cone could be represented in the coordinate system $S_c$ which is rigidly connected to the head-cutter is as follows:

$$\begin{bmatrix} x_c \\ y_c \\ z_c \\ 1 \end{bmatrix} = \begin{bmatrix} r\cos\psi - u\cos\psi_c \\ u\sin\psi_c \sin\theta \\ u\sin\psi_c \cos\theta \\ 1 \end{bmatrix} \tag{3.2.1}$$

The coordinate system $S_s$ is an auxiliary coordinate system that is also rigidly connected to the tool as mentioned earlier. The following matrix transformation is used to represent the generating surface in coordinate system $S_s$ (for a left hand gear).

$$\begin{bmatrix} x_s \\ y_s \\ z_s \\ 1 \end{bmatrix} = [M_{sc}] \begin{bmatrix} x_c \\ y_c \\ z_c \\ 1 \end{bmatrix} = \begin{bmatrix} 1 & 0 & 0 & 0 \\ 0 & \cos q & -\sin q & -s\sin q \\ 0 & \sin q & \cos q & s\sin q \\ 0 & 0 & 0 & 1 \end{bmatrix} \begin{bmatrix} x_c \\ y_c \\ z_c \\ 1 \end{bmatrix} \tag{3.2.2}$$

Equations (3.2.1) and (3.2.2) yields

$$x_s = r_c \cot\Psi_c - u \cos\Psi_c$$

$$y_s = u \sin\Psi_c \sin(\theta - q) - s \sin q$$

$$z_s = u \sin\psi_c \cos(\theta - q) + s \cos q \tag{3.2.3}$$

The unit normal to the generating surface in coordinate system $S_s$ given by [6]

$$\bar{n}_s = \frac{\bar{N}_s}{|N_s|} \quad \text{where} \quad \bar{N}_s = \frac{\partial \bar{r}_c}{\partial \theta} \times \frac{\partial \bar{r}_c}{\partial u} \tag{3.2.4}$$

From equation (3.2.4):

$$\frac{\partial r_c}{\partial \theta} = 0i + u \sin\psi_c \cos(\theta - q)\, j - u \sin\psi_c \sin(\theta - q)\, k \tag{3.2.5}$$

$$\frac{\partial r_c}{\partial u} = -\cos\psi_c\, i + \sin\psi_c \sin(\theta - q)\, j + \sin\psi_c \cos(\theta - q)\, k \tag{3.2.6}$$

using (3.2.2 ) to ( 3.2.6):

$$N_s = \begin{vmatrix} i & j & k \\ 0 & u \sin\psi_c \cos(\theta - q) & -u \sin\psi_c \sin(\theta - q) \\ -\cos\psi_c & \sin\psi_c \sin(\theta - q) & \sin\psi_c \cos(\theta - q) \end{vmatrix} \tag{3.2.7}$$

or

$$\begin{aligned} \bar{N}_s = \; & [\; u \sin^2\psi_c \cos^2(\theta - q) + u \sin^2\psi_c \sin^2(\theta - q) \;]\, i + \\ & [\; u \sin\psi_c \cos\psi_c \sin(\theta - q) \cos(\theta - q) \;]\, j + \\ & [\; u \sin\psi_c \cos\psi_c \cos(\theta - q) \;]\, k \end{aligned} \tag{3.2.8}$$

and

$$|N_s|^2 = u^2 [\sin^4\psi_c + \sin^2\psi_c \cos^2\psi_c \sin^2(\theta - q) + \sin^2\psi_c \cos^2\psi_c \cos^2(\theta - q)]$$

or

$$N_s = \sqrt{u^2 \sin^2\psi_c} = u \sin \psi_c \tag{3.2.9}$$

Therefore;

$$n_s = \frac{N_s}{|N_s|} = \sin \psi_c \, i + \cos\psi_c \, [\sin(\theta - q) \, j + \cos(\theta - q) \, k]$$

or

$$n_s = \begin{bmatrix} \sin \psi_c \\ \cos \psi_c \sin(\theta - q) \\ \cos \psi_c \cos(\theta - q) \end{bmatrix} \tag{3.2.10}$$

In order to define the unit normal with reference to the machine fixed coordinate system $S_m$ , the following procedure is used. First any surface point with respect to $S_m$ coordinate system is given by:

$$\begin{bmatrix} x_m \\ y_m \\ z_m \end{bmatrix} = [M_{ms}] \begin{bmatrix} x_s \\ y_s \\ z_s \end{bmatrix} \tag{3.2.11}$$

where

$$M_{ms} = \begin{bmatrix} 1 & 0 & 0 & 0 \\ 0 & \cos\phi_c & \sin\phi_c & 0 \\ 0 & -\sin\phi_c & \cos\phi_c & 0 \\ 0 & 0 & 0 & 0 \end{bmatrix} \tag{3.2.12}$$

The unit normal with respect to $S_m$ coordinate system is given as:

$$[n_m] = [L_{ms}] \; [n_s] \tag{3.2.13}$$

where $[L_{ms}]$ may be determined by deleting the fourth column and row in matrix (3.2.12). Thus

$$n_m = \begin{bmatrix} 1 & 0 & 0 \\ 0 & \cos\phi_c & \sin\phi_c \\ 0 & -\sin\phi_c & \cos\phi_c \end{bmatrix} \begin{bmatrix} \sin\psi_c \\ \cos\psi_c \sin(\theta - q) \\ \cos\psi_c \cos(\theta - q) \end{bmatrix} \tag{3.2.14}$$

which gives

$$n_m = \begin{bmatrix} \sin\psi_c \\ \cos\psi_c \sin\tau \\ \cos\psi_c \cos\tau \end{bmatrix} \tag{3.2.15}$$

where $\tau = \theta - q + \phi_c$ for the pinion which is a left hand gear. Note that the normal vector is a function of $\theta$ and $\phi_c$ since $q$, the cradle angle, is a constant for a given point. In figure 10, $[n]$ is seen to be the same along the cutting head cone for any $u$.

Equation (3.2.15) gives the normal vector with reference to the machine fixed coordinate system. In order to generate it with respect to the workpiece coordinate system the following transformation is carried out:

$$n_w = [M_{pm}]\ [M_{ap}] \begin{bmatrix} \sin\psi_c \\ \cos\psi_c \sin\tau \\ \cos\psi_c \cos\tau \\ 1 \end{bmatrix} \tag{3.2.16}$$

## 3.3 PROCEDURE TO DETERMINE THE INTERSECTION OF NORMAL VECTOR WITH GEAR SURFACE

After finding the normal vector with respect to the workpiece coordinate system it is required to find the intersection of the normal vector (from the pinion concave surface) with the gear convex surface. To do so the pinion concave surface (and the normal vector at the contact point) is oriented to be in mesh with the gear convex surface. During the procedure the gear convex surface is fixed because the equations to solve for the intersection point are in terms of $\mathbf{u}$, $\theta$, $\phi_c$ in $\mathbf{S_w}$. The pinion is rotated to the gear. The different rotations carried out on the pinion are described below and are shown in figure 11.

STEP 1: The pinion concave surface, with attached normal vector, are rotated by an angle such that the pinion and gear do not interfere during meshing. (Note: the algorithm produces the gear and pinion with random rotational orientation)

STEP 2: The pinion concave surface and attached normal vector are rotated by 90 degrees in counter clockwise direction about the Y axis

STEP 3: The pinion concave surface, with attached normal, are rotated by 190 degrees counter clockwise about the z axis to location 3 in figure 10 (to be near the gear convex surface). (Note that meshing actually occurs at location 2.) The rotation in step 3 to location 3 is for convenience in solving for the intersection point. This location is convenient because $u$, $\theta$, $\phi_c$ identify a gear surface point in $S_w$ at location 3.

STEP 4: The final rotation of the pinion concave surface with attached normal is a slight counter clockwise rotation about the Z axis. This is done to compensate for the rotation of the gear convex surface done to create the top land.

The procedure used to find the intersecting point is as follows:

Consider the coordinates of the contact point to be $(X_{pin}, Y_{pin}, Z_{pin})$ as shown in figure (12). Let a point in space which the normal vector passes through be given as $(Q_x, Q_y, Q_z)$ and the unit normal vector coefficients be given as $(n_x, n_y, n_z)$. Then:

$$(Q_x, Q_y, Q_z) = (X_{pin}, Y_{pin}, Z_{pin}) + b(n_x, n_y, n_z) \qquad (3.3.1)$$

where 'b' is a scalar factor.

Scale factor b is found by incrementing its value (see figure 12) such that it becomes a point on the gear convex surface. For this to happen it has to satisfy the following equations given below. The first equation is given as :

$$
\begin{aligned}
Q_x &= X_{gear} = X_{pin} + b\,(n_x) \\
Q_y &= Y_{gear} = Y_{pin} + b\,(n_y) \\
Q_z &= Z_{gear} = Z_{pin} + b\,(n_z)
\end{aligned}
\qquad (3.3.2)
$$

Any point in the gear convex surface could be found by using the relation as given below (provided the machine settings are maintained for this surface generation):

$$
\begin{bmatrix} X_{gear} \\ Y_{gear} \\ Z_{gear} \\ 1 \end{bmatrix} = [M_{wa}]\ [M_{ap}]\ [M_{pm}]\ [M_{ms}]\ [M_{sc}] \begin{bmatrix} r\cos\psi - u\cos\psi_c \\ u\sin\psi_c\sin\theta \\ u\sin\psi_c\cos\theta \\ 1 \end{bmatrix} \qquad (3.3.3)
$$

Let

$$
[M] = [M_{wa}]\ [M_{ap}]\ [M_{pm}]\ [M_{ms}]\ [M_{sc}]
$$

then using (3.3.2) and ( 3.3.3)

$$
\begin{bmatrix} X_{pin} + b\,(n_x) \\ Y_{pin} + b\,(n_y) \\ Z_{pin} + b\,(n_z) \\ 1 \end{bmatrix} = [M] \begin{bmatrix} r\cos\psi - u\cos\psi_c \\ u\sin\psi_c\sin\theta \\ u\sin\psi_c\cos\theta \\ 1 \end{bmatrix} \quad \ldots\ldots\ldots\ldots\ldots (3.3.4)
$$

or

$$[M] \begin{bmatrix} r\cos\psi - u\cos\psi_c \\ u\sin\psi_c\sin\theta \\ u\sin\psi_c\cos\theta \\ 1 \end{bmatrix} - \begin{bmatrix} X_{pin} + b\,(n_x) \\ Y_{pin} + b\,(n_y) \\ Z_{pin} + b\,(n_z) \\ 1 \end{bmatrix} = 0 \qquad (3.3.5)$$

From equation (3.3.5) three equations could be obtained such that

$$A_1(\Phi, b, u) = A_2(\Phi, b, u, \theta) = A_3(\Phi, b, u, \theta) = 0 \qquad (3.3.6)$$

By using the equation of meshing given in equation (2.2.1) along with the three other equations given in (3.3.6), the unknowns **u**, $\theta$, $\phi_c$, and **b** can now be solved for. These values of **u**, $\theta$, $\phi_c$, **b** will now define the intersection of the normal vector with the gear convex surface. The same procedure is adopted to find the intersection of all vectors (parallel to the contact point normal, and from grid points on the pinion concave surface) with the gear convex surface. Later, these intersecting points are rotated in TDGMP [8] so as to lie on the gear convex surface in mesh. The following rotations are carried out:

STEP 1: The intersection points are rotated by an angle required to create the top land of the gear surface about Z axis.

STEP 2: Later these points are rotated by $(360/N_t) + 180$ degrees in the counter clockwise direction to lie on the surface of gear convex surface in mesh.

The intersecting points which do not lie within the boundary of the gear convex surface are discarded. Note that while doing this care should be taken so as not to create excessive distortion of the hex elements on the gear.

## 3.4 VERIFICATION OF THE INTERSECTION POINT

To check the results of the procedure adopted earlier, the following method is used. The $(\mathbf{u}, \theta, \phi_c)$ values obtained at the intersection of the gear convex surface is transformed into $(\mathbf{X_{gear}}, \mathbf{Y_{gear}}, \mathbf{Z_{gear}})$ values using the coordinate transformation given below. Note that initial machine parameters for the gear convex surface generation should be used during this transformation. This is given by equation (3.3.3) which is:

$$\begin{bmatrix} X_{gear} \\ Y_{gear} \\ Z_{gear} \\ 1 \end{bmatrix} = [M_{wa}]\ [M_{ap}]\ [M_{pm}]\ [M_{ms}]\ [M_{sc}] \begin{bmatrix} r\cos\psi - u\cos\psi_c \\ u\sin\psi_c \sin\theta \\ u\sin\psi_c \cos\theta \\ 1 \end{bmatrix}$$

The result obtained is now substituted back in equation (3.3.2)

$$X_{gear} = X_{pin} + b\,(n_x)$$
$$Y_{gear} = Y_{pin} + b\,(n_y)$$
$$Z_{gear} = Z_{pin} + b\,(n_z)$$

The value of ( $X_{gear}$, $Y_{gear}$, $Z_{gear}$ ) obtained, if same, verifies the point at which the normal vector pierces the gear convex surface and is the intersection point of interest.

The above method is used to locate the intersection of normals from all points on the pinion surface (in the contact zone) with the gear surface. The gear tooth surface is remeshed utilizing the intersection points as shown in figure 13. GAP elements are connected between corresponding nodal points on the pinion and the intersection points on the gear surface.

# CHAPTER IV

# NUMERICAL EXAMPLES

This chapter describes a numerical example to determine the values of the contact stresses of spiral bevel gearset using an example design. Three different models of these gears at different levels of difficulty are analyzed. The first model simulates a two tooth contact, one pinion and one gear tooth. The second model simulates two contact points using four gear teeth and three pinion teeth. The third model simulates the two contact points along with added hub effects. Various contact stress levels are discussed.

## 4.1 MODEL DESCRIPTIONS

All models were constructed in a TDGMP [8] from the output of the computer programs and were analyzed for contact stress distribution using a finite element program [9]. A non-linear static analysis solution technique with GAP elements is used for the analysis. The modeling was done on a workstation and the analysis was done via a supercomputer. The models where constructed using 8 noded HEX elements and 2 noded GAP elements.

MODEL I: The first model contains one pinion and one gear tooth as shown in figure (14). The model consists of 1280 elements and 1980 nodes. (5940 degrees of freedom). The torque load was applied as a concentrated force in the beam as shown. In all of the models; the pinion was fixed by specifying zero displacement on the four corner nodes of each rim face, 8 nodes total were fixed in this manner; and the gear was free to rotate about its axis of rotation (Z axis).

Model I contains 15 GAP elements along the contact area. Initially, only one is closed. This simulates the contact condition in the model. The beam section has a very high modulus to prevent excessive bending. The various stress results obtained are as shown in figures (15-18). The solution iterates 5 times to confirm the assumption on the GAP elements (i.e. open or closed) is in agreement with the finite element displacement solution. The structure of the contact area and the history of the GAP elements at each iteration is given in figure (19).

The values of the minimum element principal stresses as plotted by the TDGMP [8] and the average values of the minimum principal stresses at various nodes in the contact area is shown in table (I).

MODEL II: This model contains four gear teeth and three pinion teeth in mesh. The model consists of 7626 nodes and 5292 hex elements. (22878 degrees of freedom). The contact

stresses at two different contact regions are analized with this model. A metal hub is provided on the gear to transmit the forces to the two different contact areas. The model generated and the boundary conditions imposed are as shown in figure (20). The model contains 15 GAP elements in the major contact region and 6 on the edge contact region.

The GAP elements in the major contact region are located using the algorithms described in this report. At the edge contact, the GAP elements are located by plotting lines from the pinion surface and finding the intersection point with the gear surface with the TDGMP [8]. In both contact regions one GAP element is initially closed and the rest are open. The solution iterated 4 times to reach equilibrium. The status of the GAP elements after every iteration is shown in figure (29). The values of the minimum principal stresses and the average minimum nodal principal stresses are given in table (II). The stress contours are also shown in figures (21-28).

MODEL III: This model contains four gear teeth and three pinion teeth, similar to Model II, with the added hub region as shown in figure (30). It contains 10101 nodes and 7596 elements (30303 degrees of freedom) The model contains 15 GAP elements in the first contact region and 6 in the edge contact. As in MODEL II one GAP element in both the contact regions is closed initially, and the others open. The

solution iterated 3 times before obtaining the final solution on the fourth iteration. Different stress contours are shown in figures 31-34. The status of each GAP element after each iteration is shown in figure 35. Table III gives the element minimum principal stress values and the average nodal minimum principal stress values.

For all three models the torque is applied as a force at a moment arm of 2.0976 inches. Hence, the total torque applied on the gear is approximately 9911 inch pounds. The pinion torque is three times less or 3303 inch pounds.

# CHAPTER V

## DISCUSSION OF RESULTS

MODEL I: This model consists of one gear tooth and one pinion tooth with minimal hub. In this model the element minimum principal contact stress on the pinion is found to be around -195,923 psi. This value occurs at the node connected by GAP element 1231 as shown in figure (19). The average nodal minimum principal stresses showed a higher value of about 380,000 psi, and with a maximum of 447,700 psi.. The maximum influence of average nodal minimum principal stress is at the node connecting GAP element 1228. Six GAP elements are closed in the final iteration.

The nodal stresses are higher because they occur at the GAP elements which acts like a concentrated force applied directly to a node. The elemental stresses are based on nodal averages and, as a result, are lower than the nodal stresses.

Model II: This model was created to distribute the load to a second pair of teeth in contact. The minimum element principal stresses at the major contact region was found to be -156,041 psi. The average nodal minimum principal stress is found to be around -300,000 psi. The maximum influence is at the node connected by GAP element 1232 (see figure 29)

which showed a value of -339,064 psi. The stresses decrease, compared to Model I, because of load distribution to the edge contact region.

At the edge contact, the minimum principal element stress is found to be around -101,661 psi and the average nodal stresses are found to be about -220,000 psi. The maximum average nodal minimum principal stress value was concentrated at the node connected by GAP element 6200 (see figure 29) is around -435,002 psi.

The GAP element status at each iteration shows that initially 9 GAP element at the major contact area and 1 at the edge contact are closed. Also at the time of convergence, 5 in the major contact area and 1 in the edge contact area are closed. The 5 GAP elements closed were also closed in the final iteration of model I.

Model III: This model also consists of four gear teeth and three pinion teeth in mesh. Also modeled is a bigger section of hub.(see figure 30) The minimum principal element stress obtained from the TDGMP [8] is found to be -123,967 psi. The mean nodal principal stresses obtained at the contact region is found to be 260,000 psi. The maximum influence is at node connecting, GAP element 1232 (see figure 35) and the value is -299,931 psi. At the edge contact region, the minimum principal element stress is found to be around -84,932 psi. The mean of the average nodal minimum principal stresses in

the contact region is found to be -200,000 psi. The maximum influence is at node connected by GAP element 6200 ( see figure 35) and it is -363,720 psi. These results are consistent with estimates of hertzian contact stresses for these gears.

At the end of the first iteration, 8 GAP elements in the major contact area and 1 in the edge contact area are closed and after the final iteration 4 in the major contact area and 1 in the edge contact area are closed. The same GAP elements closed in the major contact region were also closed in Models I and II.

For this model the area of the contact region is marked as shown in figure 36. To estimate the area the average area due to the influence of each GAP element is taken as shown in figure (37). The area of each rectangle is found to be 0.0049 sq. in. Hence, the area of the entire contact region is 4 x 0.0049 which equals 0.0196 square inch.in*in.

For all three models, large node to node stress variation indicates a need for mesh refinement.

# CHAPTER VI

# CONCLUSIONS

The authors presented a method for doing nonlinear finite element contact stress analysis of spiral bevel gears. The method incorporates the following features.

1) A model was developed for obtaining spiral bevel gear surface points. This model is based on numerical analysis of the manufacturing kinematics.

2) The gear and pinion are orientated for mesh with a series of coordinate transformations.

3) The gear surface is remeshed to provide proper orientation of the GAP elements used to simulate contact.

4) A series of models were analyzed with increased complexity.

   A) Model I - One pinion and one gear tooth in mesh, (5940 degrees of freedom)

   B) Model II - Four gear teeth and three pinion teeth in mesh. (22878 degrees of freedom)

   C) Model II - Four gear teeth and three pinon teeth in mesh with added hub region. (30303 degrees of freedom)

5) Results agreed well with calculated Hertzian contact stresses.

6) Large node to node stress variation indicate a need for refinement.

## REFERENCES


1. Chao, H. C., Baxter, M, and Cheng, H. S., A Computer Solution for the Dynamic Load, Lubricant Film Thickness and Surface Temperatures in Spiral Bevel Gears. Advanced Power Transmission Technology, NASA CP-2210, AVRADCOM TR-82-C-16, 1981, PP345-364.

2. Drago, R. J., and Uppaluri, B. R., Large Rotorcraft Transmission Technology Development Program, Vol. I, Technical Report. (D210-11972-1-VOL-1, Boeing Vertol Co., NASA Contract NAS3-22143) NASA CR-168116, 1983.

3. Handschuh, R. F., and Litvin, F. L., A Method of Determining Spiral-Bevel Gear Tooth Geometry for Finite Element Analysis, NASA TP-3096, AVSCOM TR 91-C-020, 1991.

4. Litvin, F. L., and Lee, H. T., Generation and Tooth Contact Analysis of Spiral Bevel Gears With Predesigned Parabolic Functions of Transmission Errors. NASA CR-4259, AVSCOM TR 89-C-014, 1989.

5. Litvin, F. L., "Theory of Gearing" NASA RP-1212, 1989.

6. Litvin, F. L., Tsung, W. J., and Lee, H. T., Generation of Spiral Bevel Gears with Conjugate Tooth Surfaces and Tooth Contact Analysis. NASA CR-4088, AVSCOM TR 87-C-22, 1987.

7. Burden, R. L., and Faires, J. D., Numerical Analysis, 3rd edition, Prindle, Weber & Schmidt, 1985.

8. PATRAN Users Manual, PDA Engineering, Costa Mesa, CA. 1991.

9. MSC-NASTRAN Users Manual, MacNeal Schwendler Corporation, Los Angeles, CA 1990.

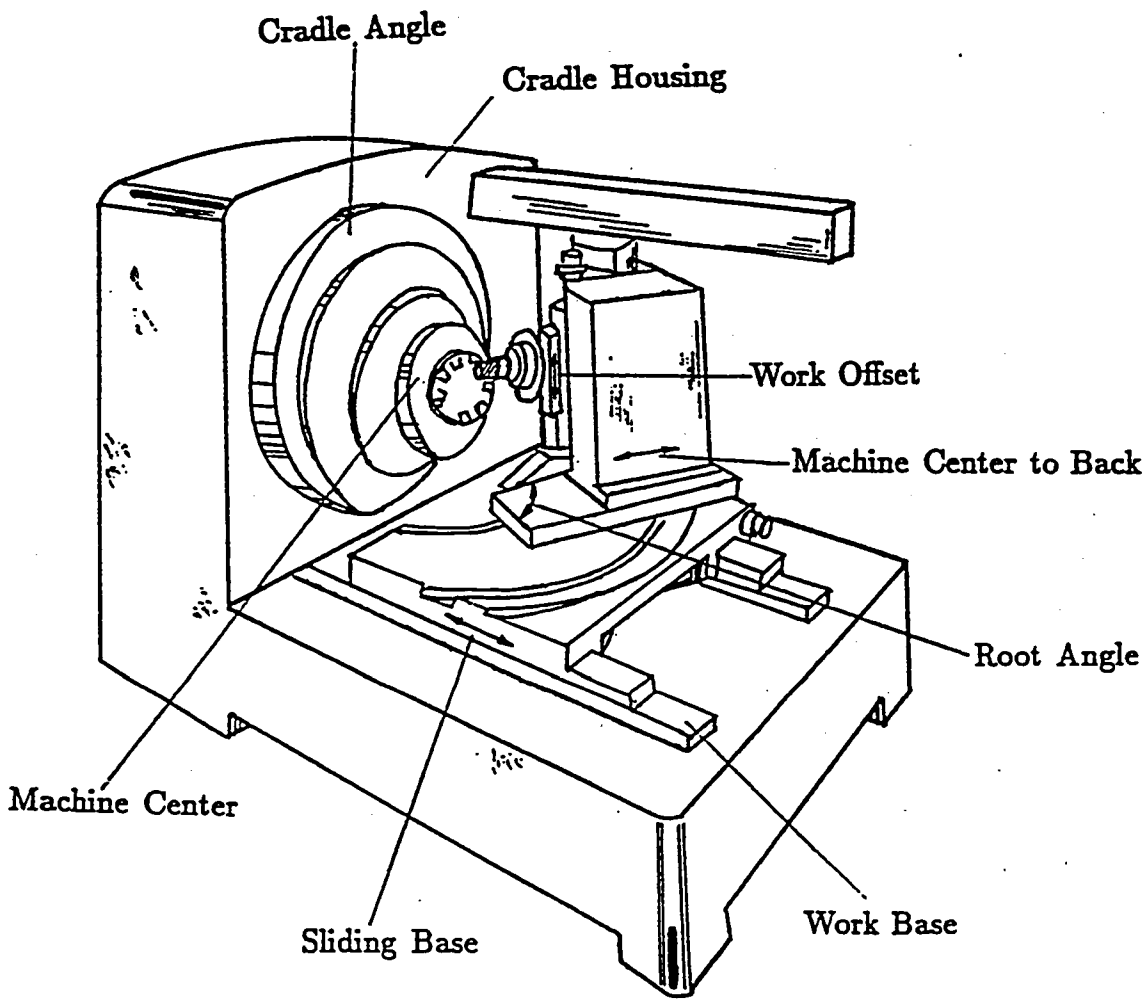


Figure 1. - Machine used to generate spiral bevel gear surface. [4]

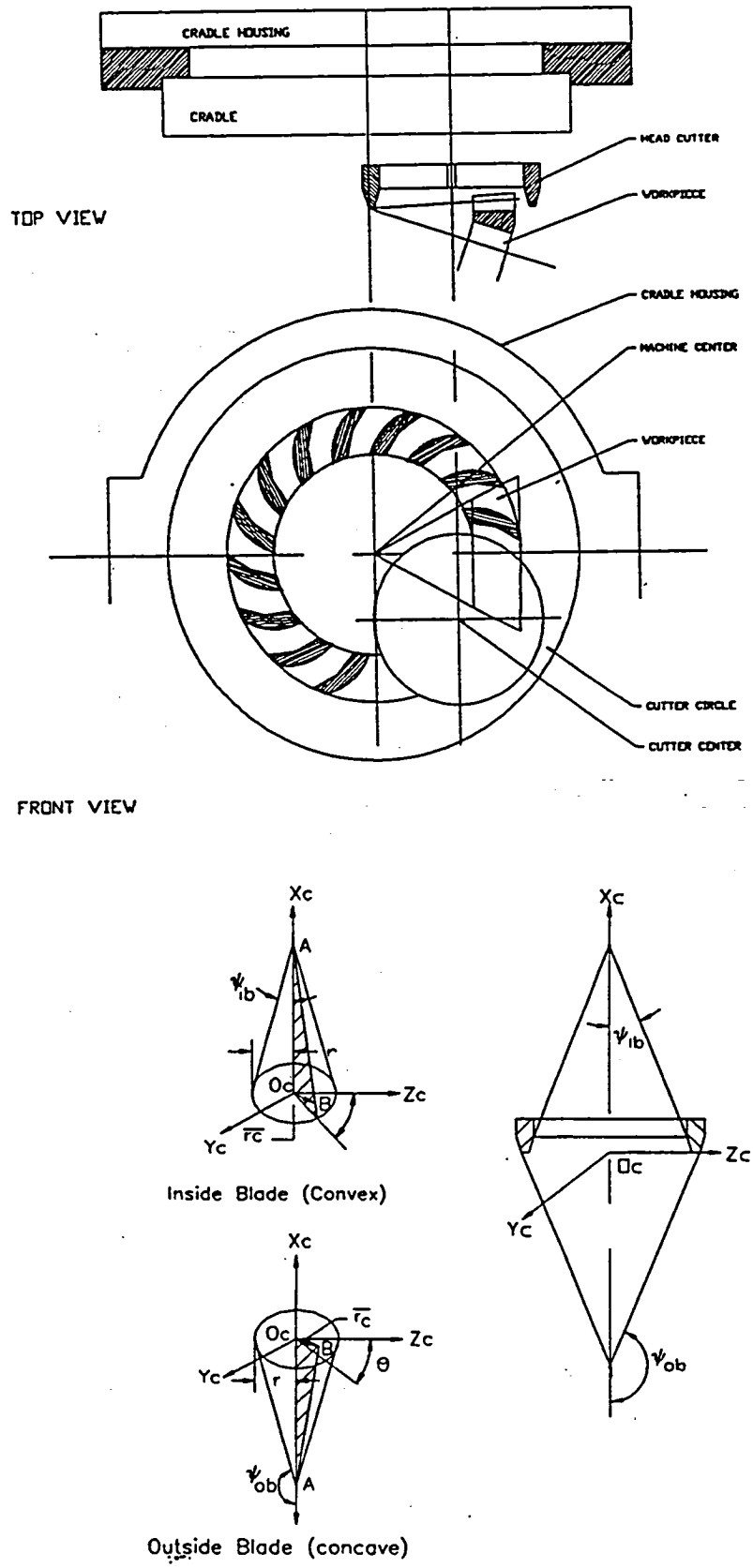


Figure 2 - Machining process with workpiece and cutter orientations.

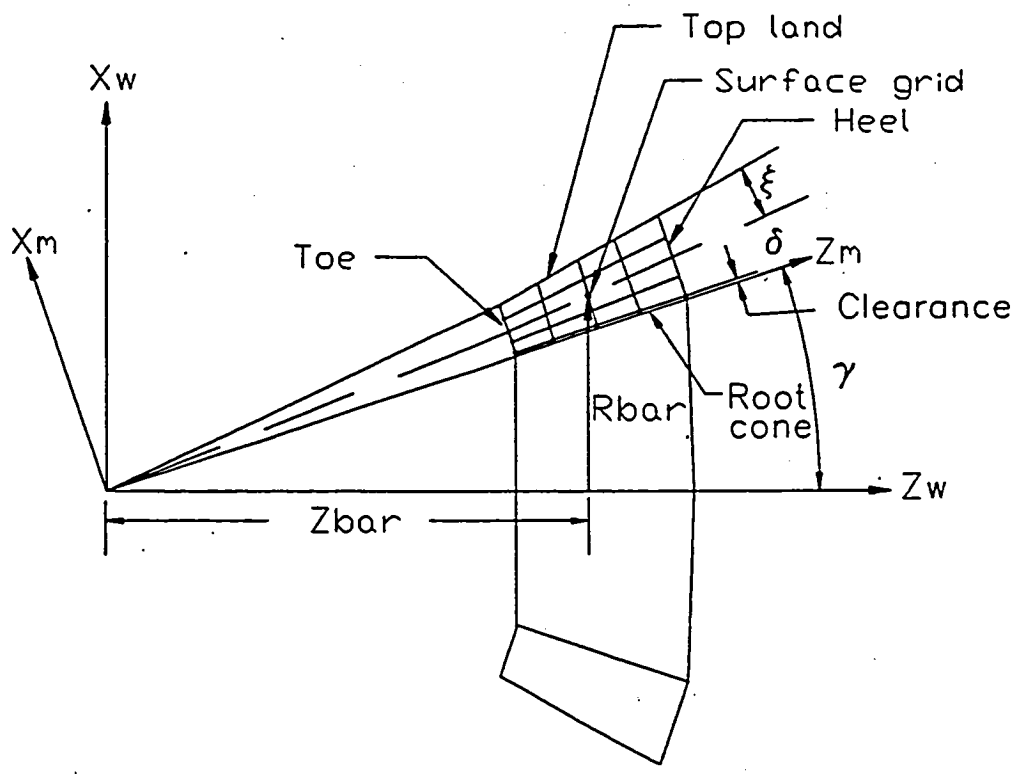


Figure 3 - Projection of gear tooth into XY plane

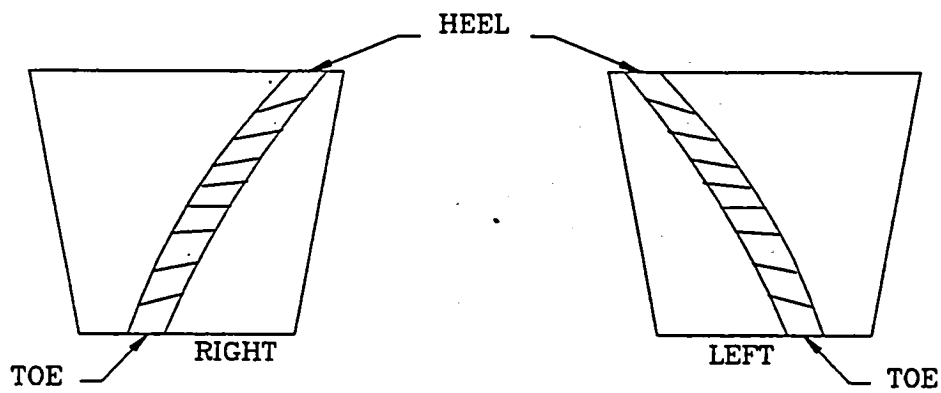


Figure 4. - Right and left hand spiral bevel gears.

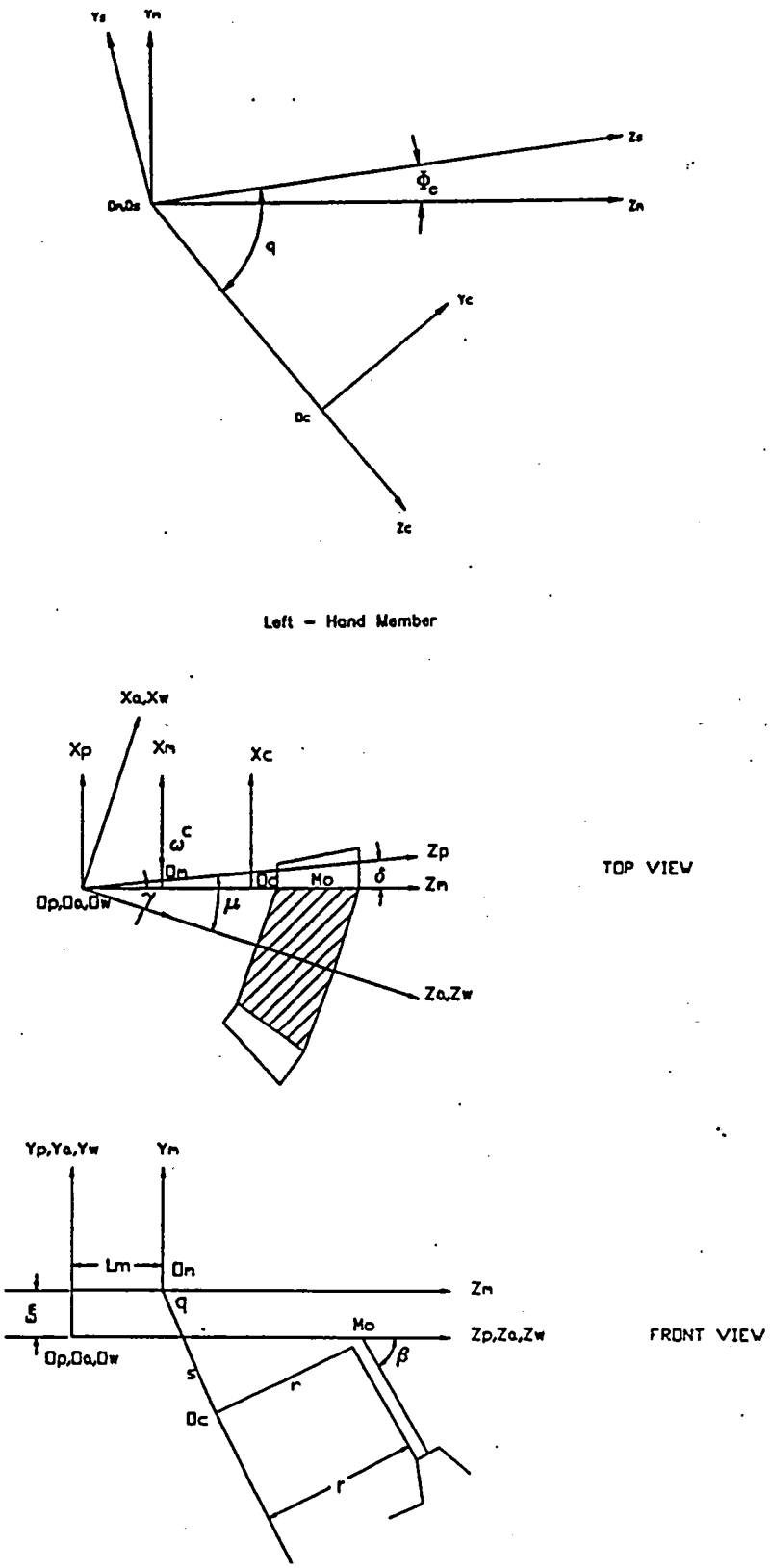


Figure 5. - Orientation of Coordinate system for cutter, cradle and system fixed to machine frame.

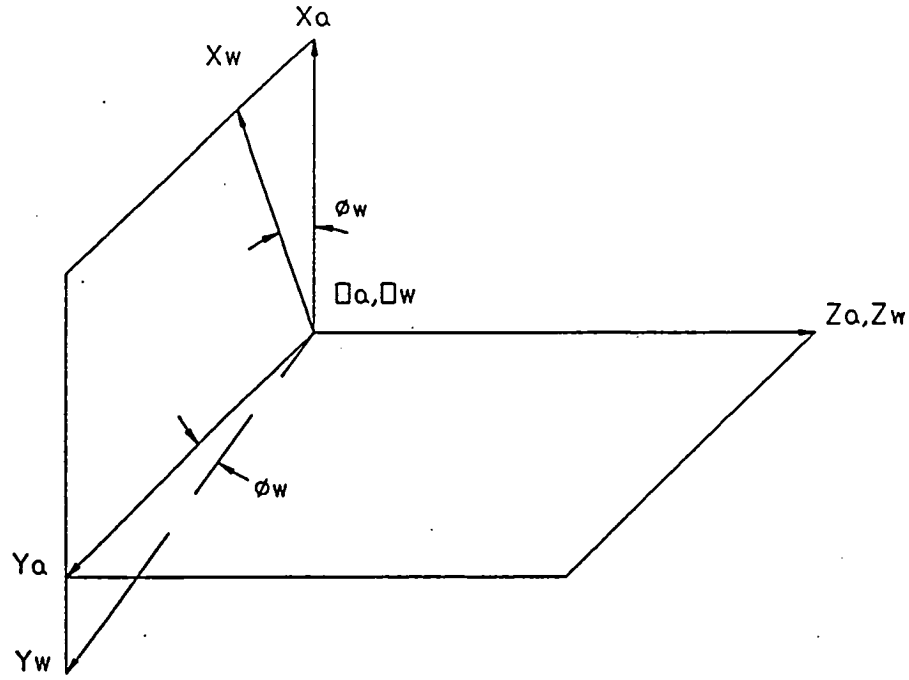


LEFT HAND MEMBER

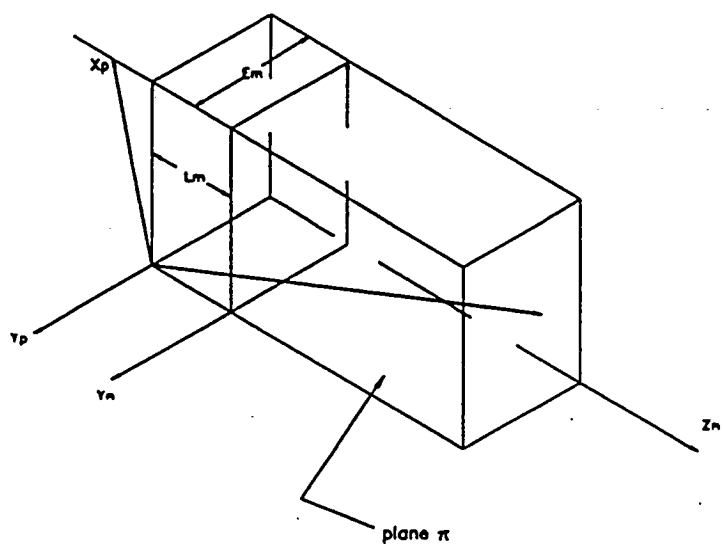


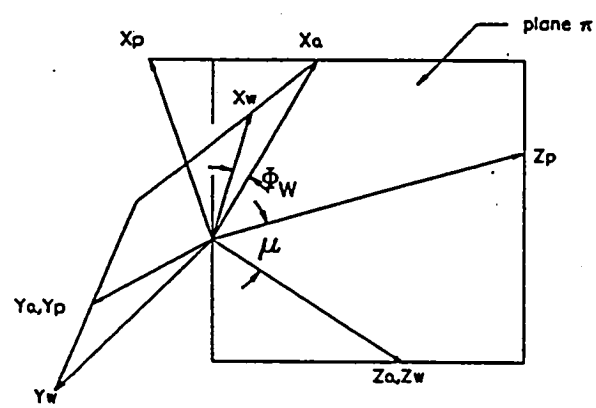


Figure 6 - Machine settings and orientation with rotation of workpiece during tooth surface generation

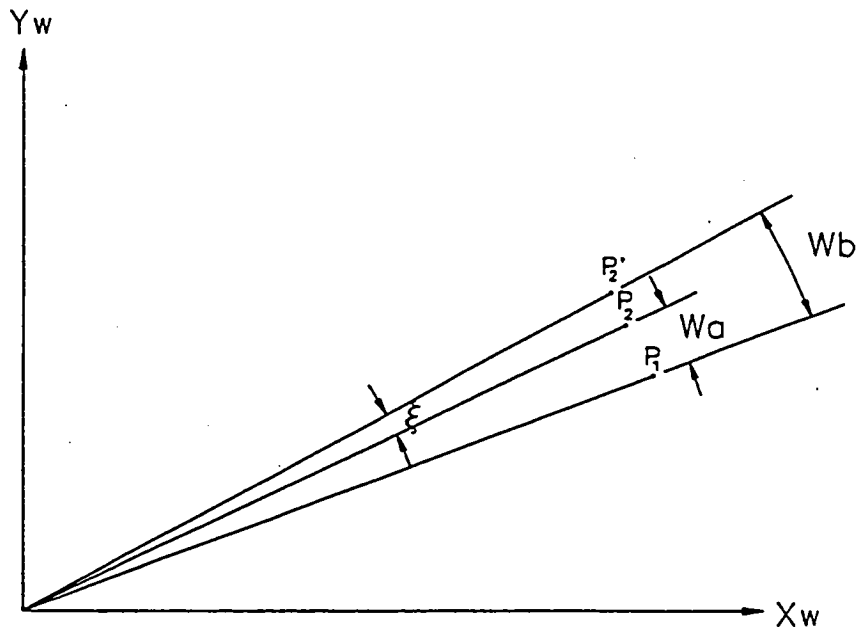


Figure 7. - Concave and convex orientations required to obtain desired top land thickness.

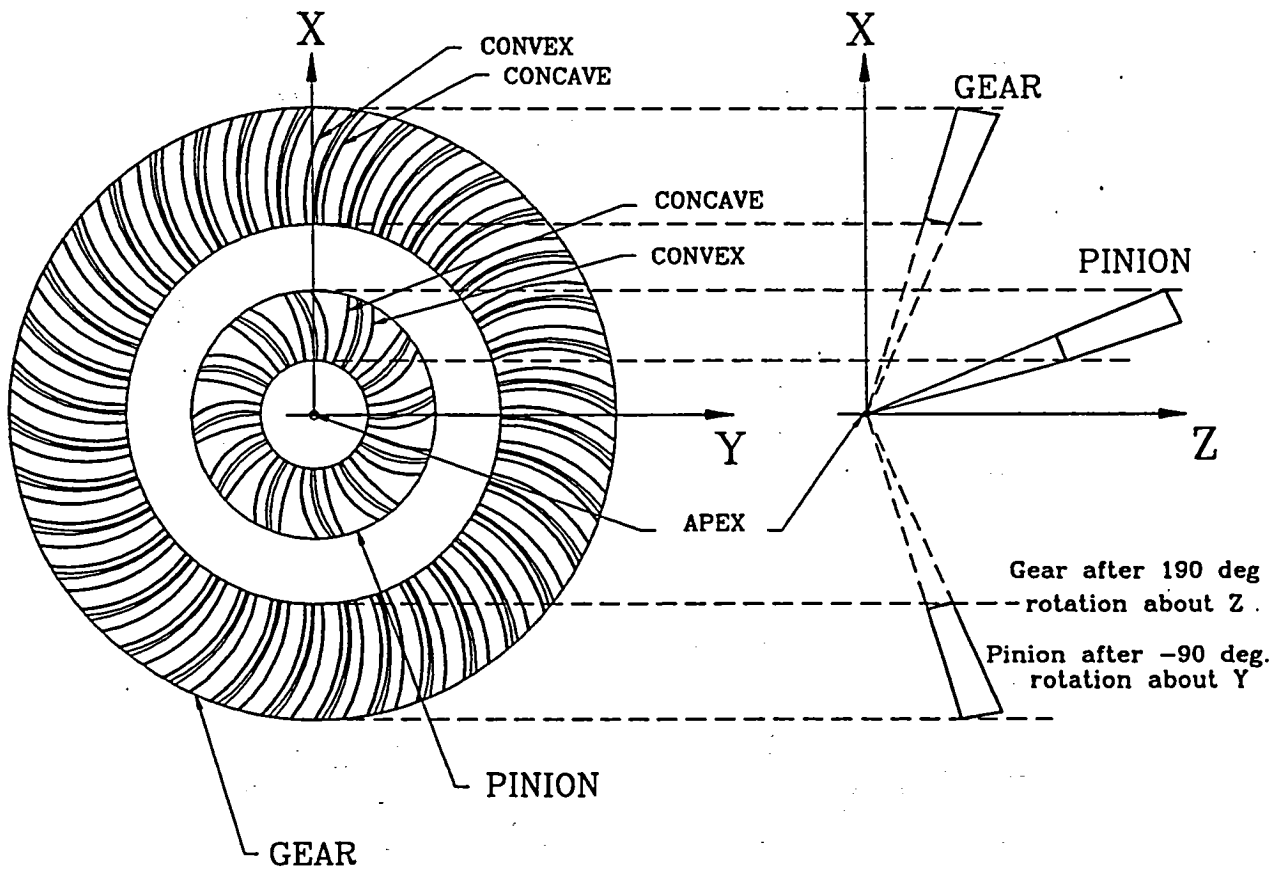


Figure 8. - Gear and pinion orientations required for meshing.

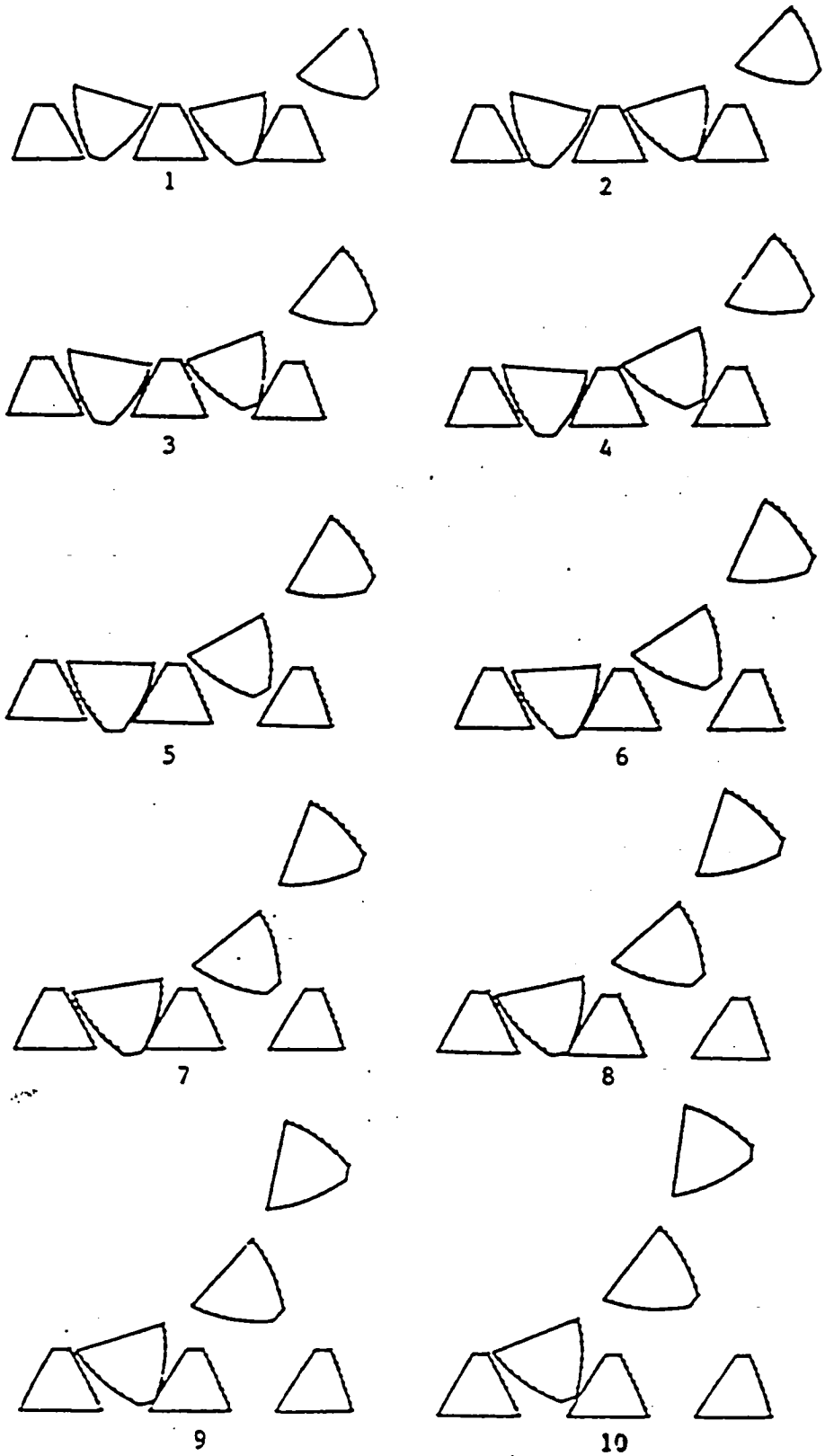


Figure 9. - Different sections taken along the pinion spiral. Used to determine contact point.

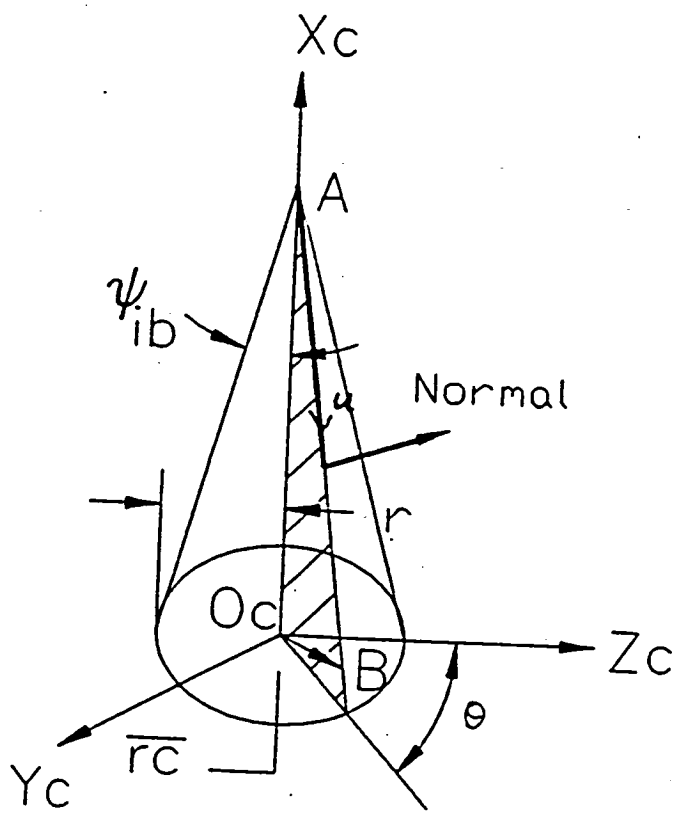


Figure 10. - Cutting head cone surface normal.

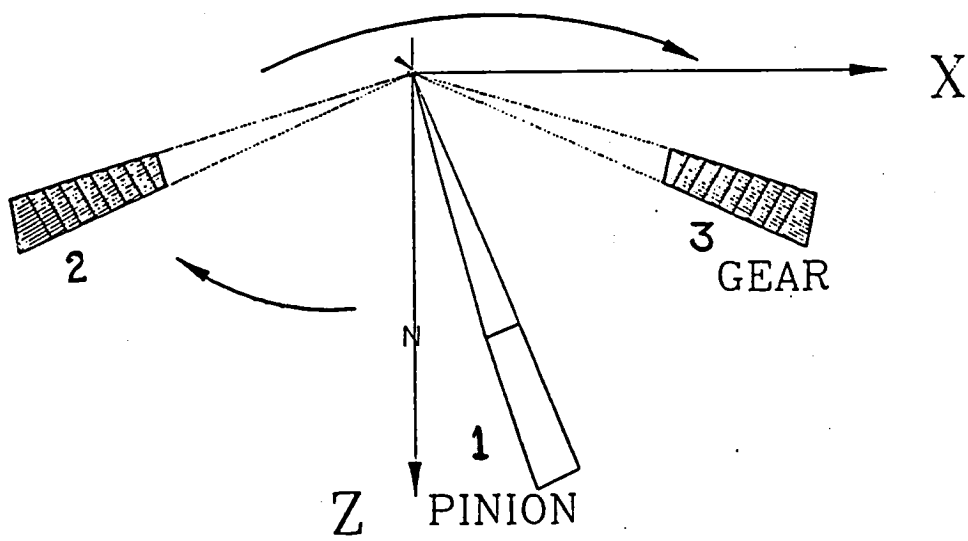


Figure 11. - Rotations required to solve for intersection of pinion normals with gear surface. Location 1: Small rotation about Z axis (prevents interference during meshing). Location 2: -90 degree rotation about Y axis. Location 3: -190 degree rotation about Z axis to place pinion in mesh with gear. Also; small rotation of gear convex surface about Z axis to create top land.

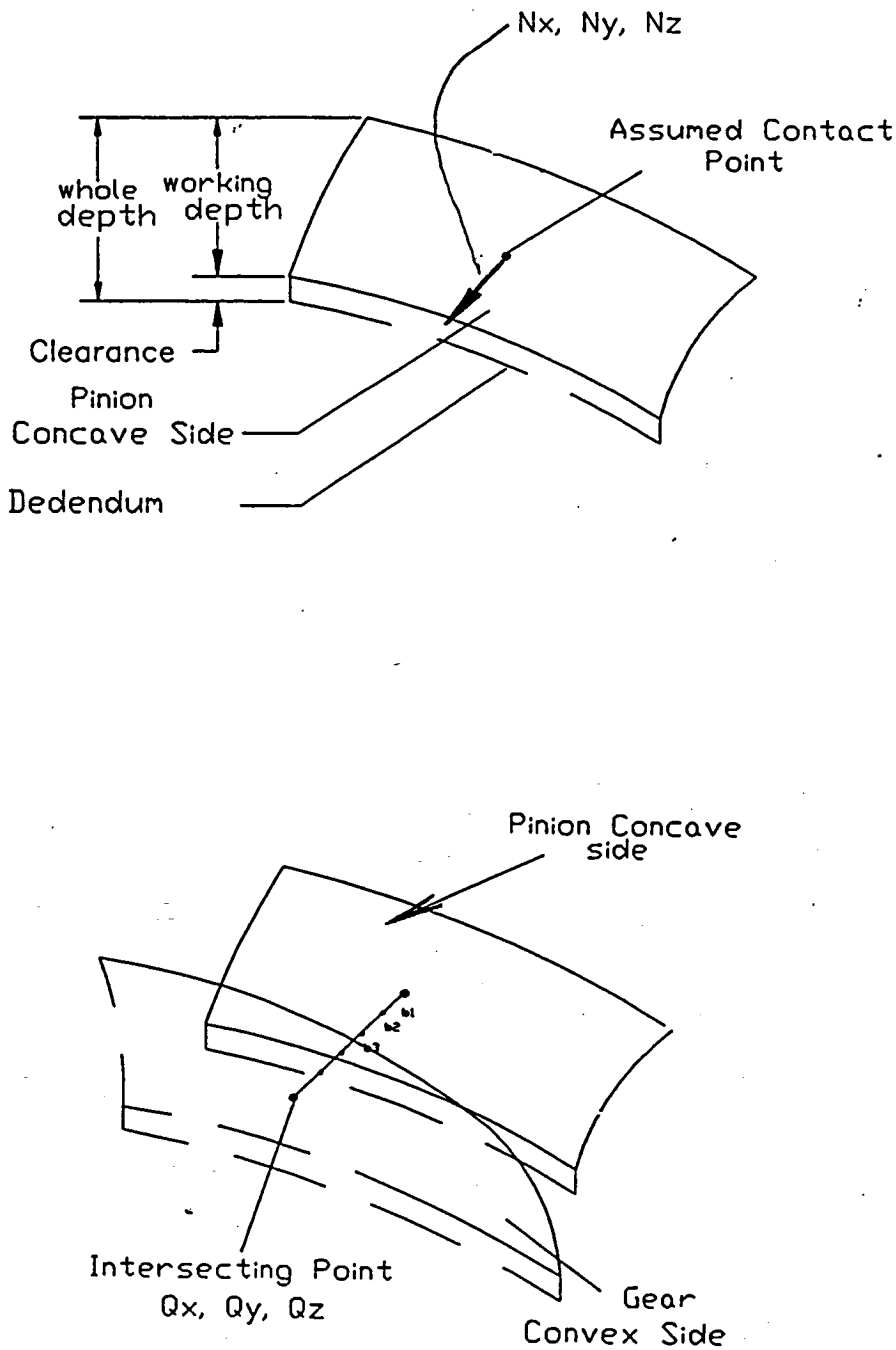


Figure 12. - Illustration of normal from pinion intersecting gear convex surface.

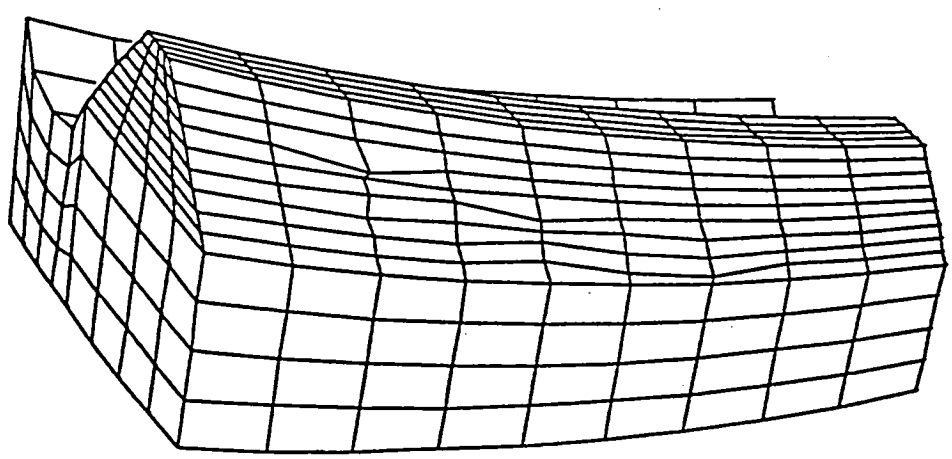

Figure 13. - Gear geometry distortion after connecting gap elements.

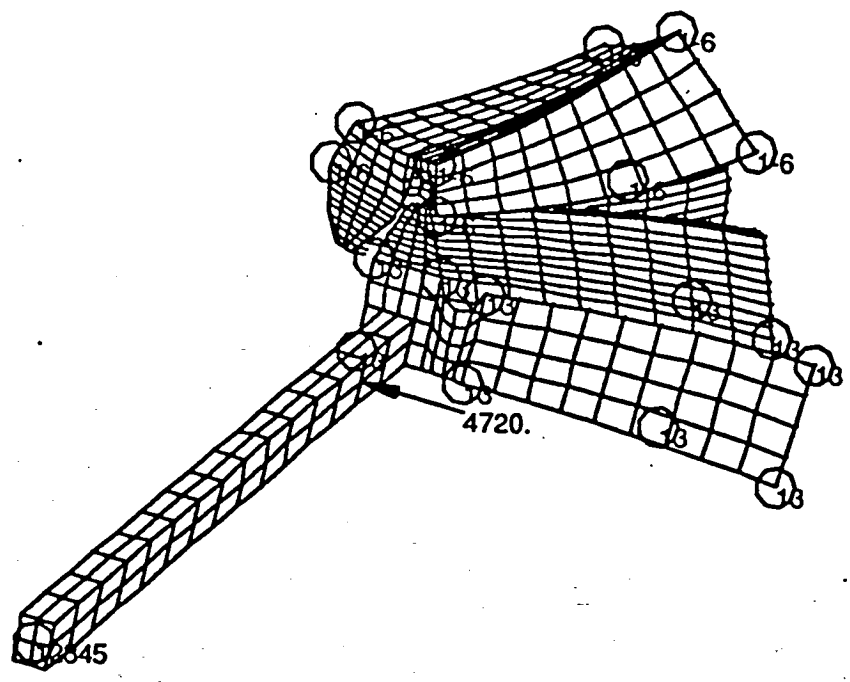


Figure 14. - Model I; pinion and gear tooth in mesh with boundary conditions.

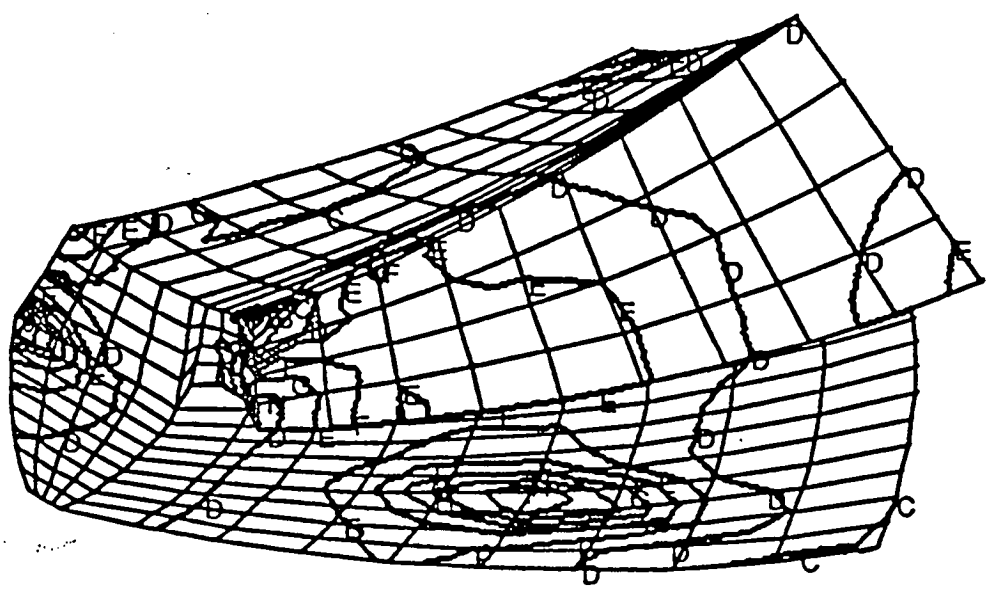

| | Psi |
|---|---|
| A | 50447. |
| B | 22332. |
| C | -5782. |
| D | -33896. |
| E | -62010. |
| F | -90124. |
| G | -118239. |
| H | -146353. |
| I | -174467. |
| J | -202581. |

Figure 15. - Model I; minimum principal element stresses in pinion tooth.

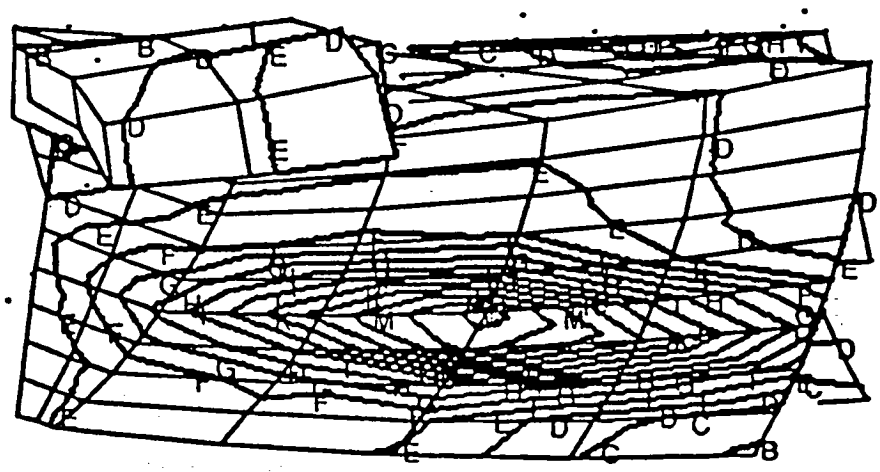

| | Psi |
|---|---|
| A | -6496. |
| B | -19560. |
| C | -32624. |
| D | -45688. |
| E | -58752. |
| F | -71816. |
| G | -84880. |
| H | -97944. |
| I | -111008. |
| J | -124072. |
| K | -137136. |
| L | -150200. |
| M | -163264. |
| N | -176328. |
| O | -189393. |

Figure 16. - Model I; Minimum principal element stresses in pinion.

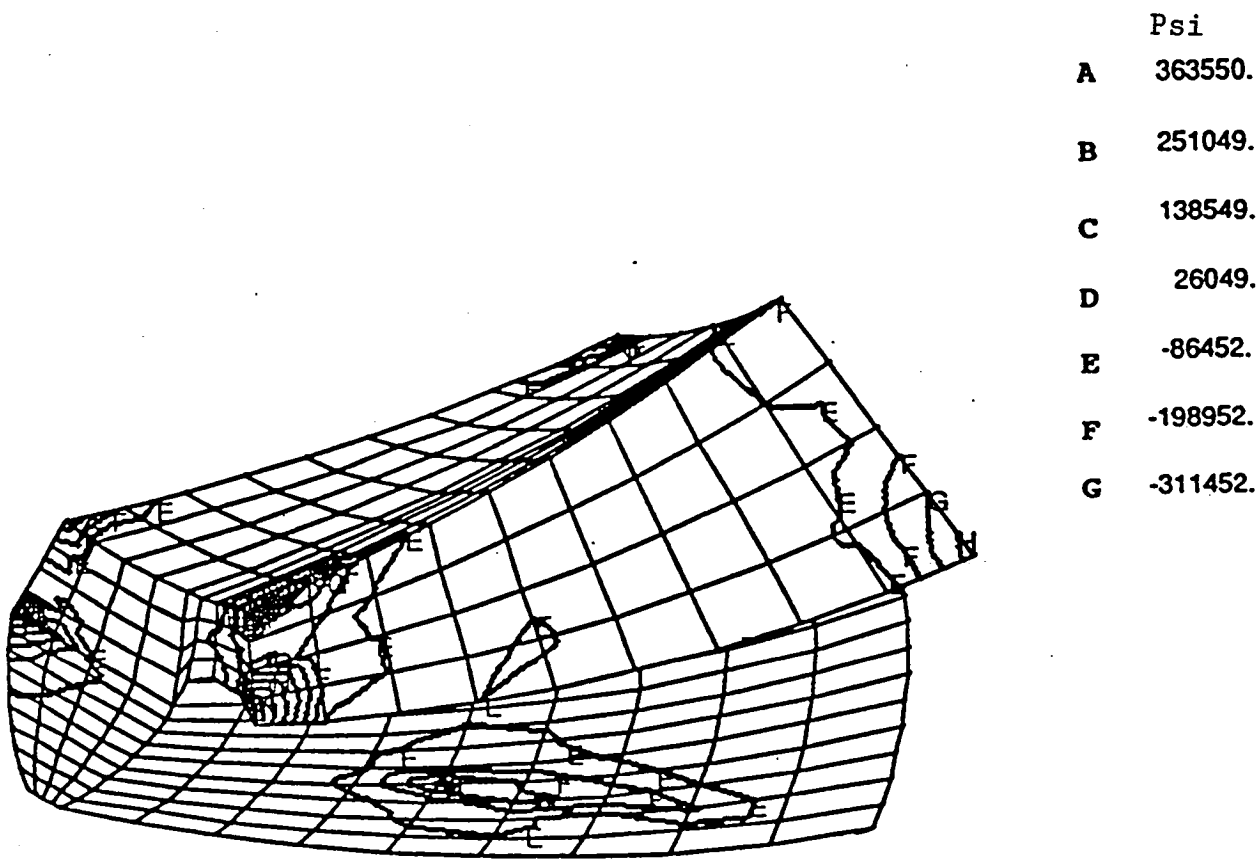


Figure 17. - Model I; average nodal minimum principal stresses in pinion tooth.

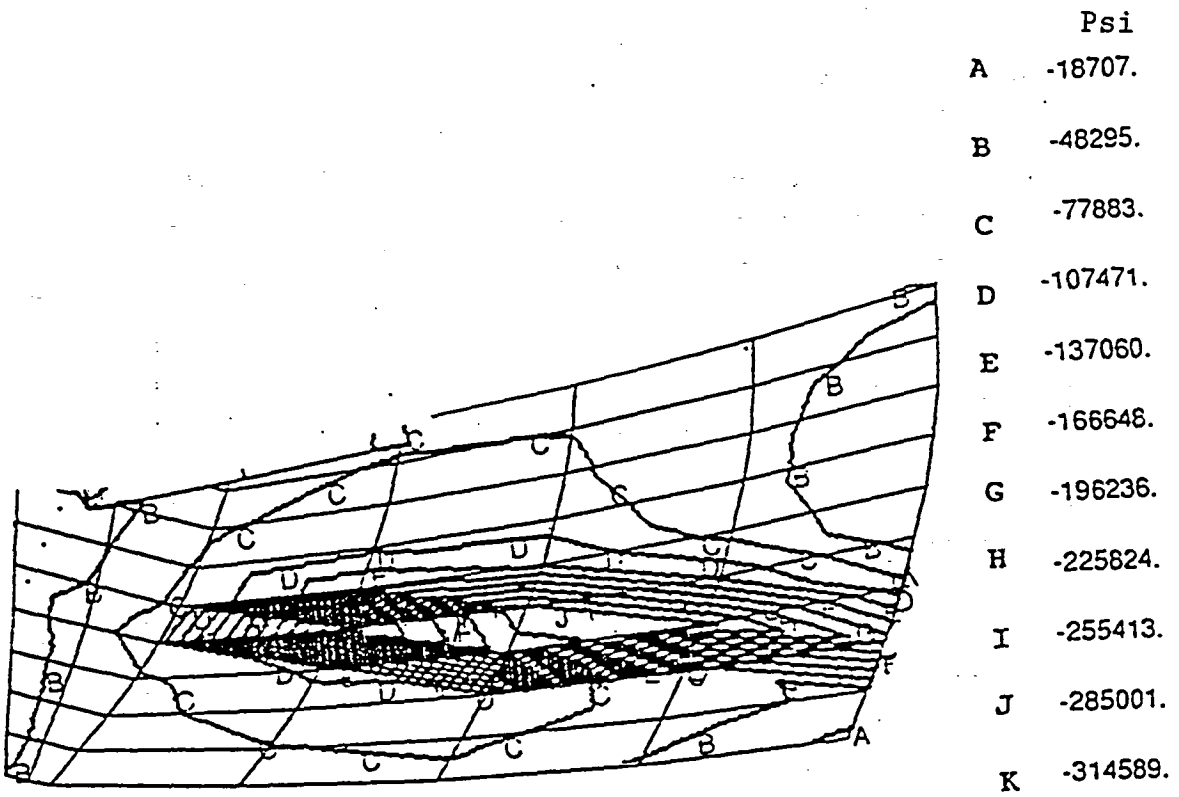


Figure 18. - Model I; average nodal minimum principal stresses in pinion at contact region.

GAP ELEMENTS AT THE CONTACT REGION

| | | | | |
|---|---|---|---|---|
| ⊙ 1225 | ⊙ 1228 | ⊙ 1231 | • 1234 | • 1237 |
| • 1226 | • 1229 | ⊙ 1232 | ⊙ 1235 | • 1238 |
| • 1227 | • 1230 | • 1233 | • 1236 | ⊙ 1239 |

• GAP element number at the contact area
⊙ Closed GAP element number at the last iteration

GAP ELEMENTS CLOSED AFTER EACH ITERATION

| ITERATION 1 | ITERATION 2 | ITERATION 3 | ITERATION 4 | ITERATION 5 |
|---|---|---|---|---|
| 1225 | 1225 | 1225 | 1225 | 1225 |
| 1226 | 1228 | 1228 | 1228 | 1228 |
| 1228 | 1229 | 1231 | 1231 | 1231 |
| 1229 | 1231 | 1232 | 1232 | 1232 |
| 1230 | 1232 | 1233 | 1235 | 1235 |
| 1231 | 1233 | 1235 | 1239 | 1239 |
| 1232 | 1235 | 1239 | | |
| 1233 | 1239 | | | |
| 1234 | | | | |
| 1235 | | | | |
| 1238 | | | | |
| 1239 | | | | |

FIGURE 19.- Model I: GAP element status at each iteration.

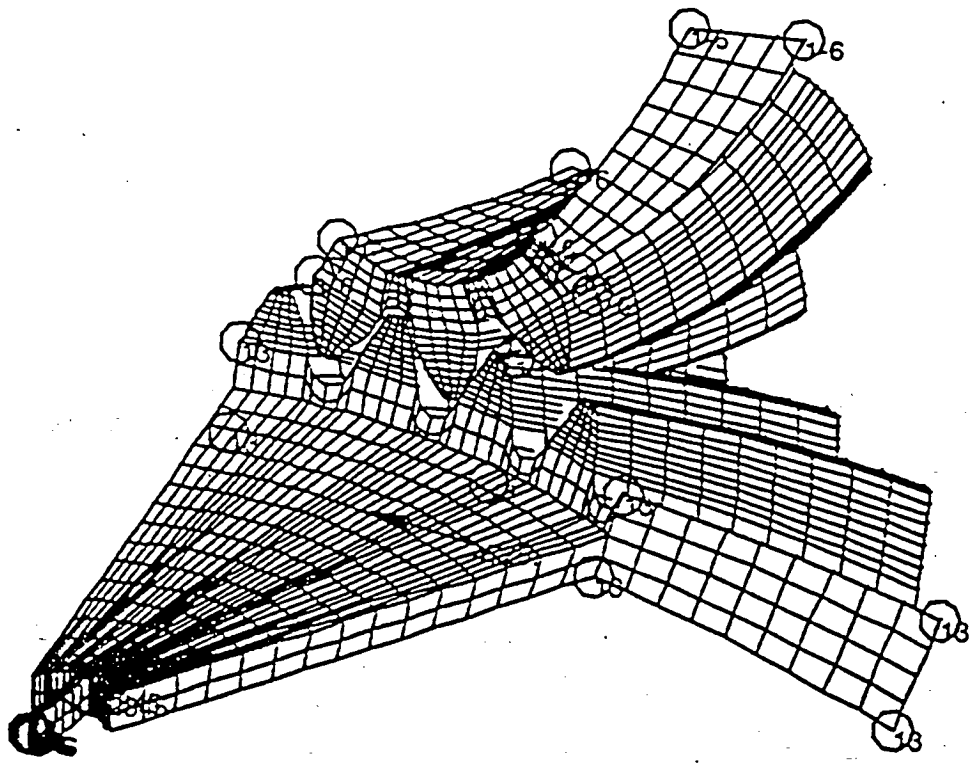

Figure 20. - Model II. Mesh generation with boundary conditions.

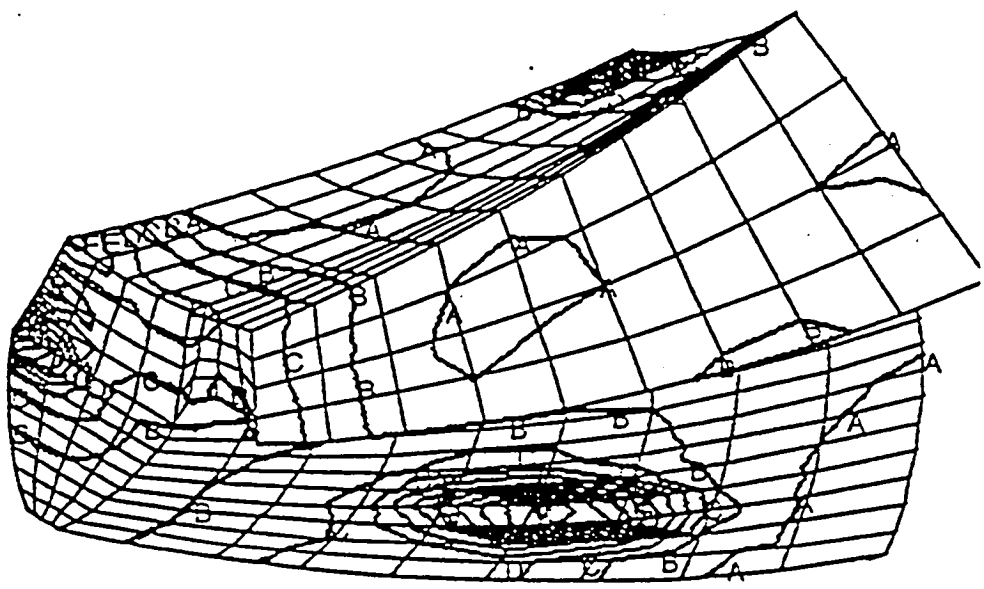

| | Psi |
|---|---|
| A | -7564. |
| B | -22181. |
| C | -36797. |
| D | -51414. |
| E | -66031. |
| F | -80647. |
| G | -95264. |
| H | -109880. |
| I | -124497. |
| J | -139113. |
| K | -153730. |
| L | -168347. |
| M | -182963. |
| N | -197580. |
| O | -212196. |

Figure 21. - Model II. Minimum principal element stresses in pinion having major contact.

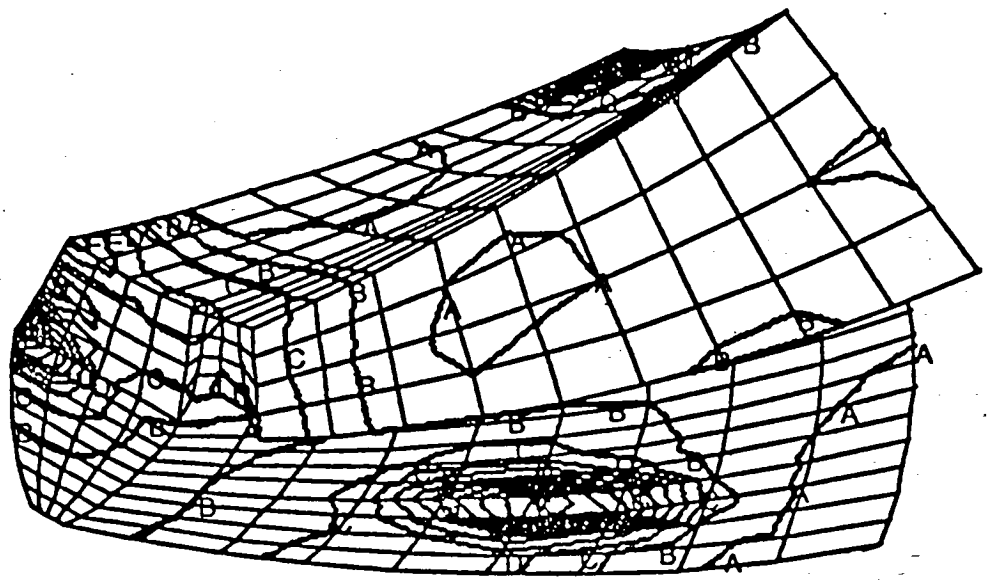

| | Psi |
|---|---|
| A | -7564. |
| B | -22181. |
| C | -36797. |
| D | -51414. |
| E | -66031. |
| F | -80647. |
| G | -95264. |
| H | -109880. |
| I | -124497. |
| J | -139113. |
| K | -153730. |
| L | -168347. |
| M | -182963. |
| N | -197580. |
| O | -212196. |

Figure 22. - Model II; minimum principal element stresses at major contact region of pinion tooth.

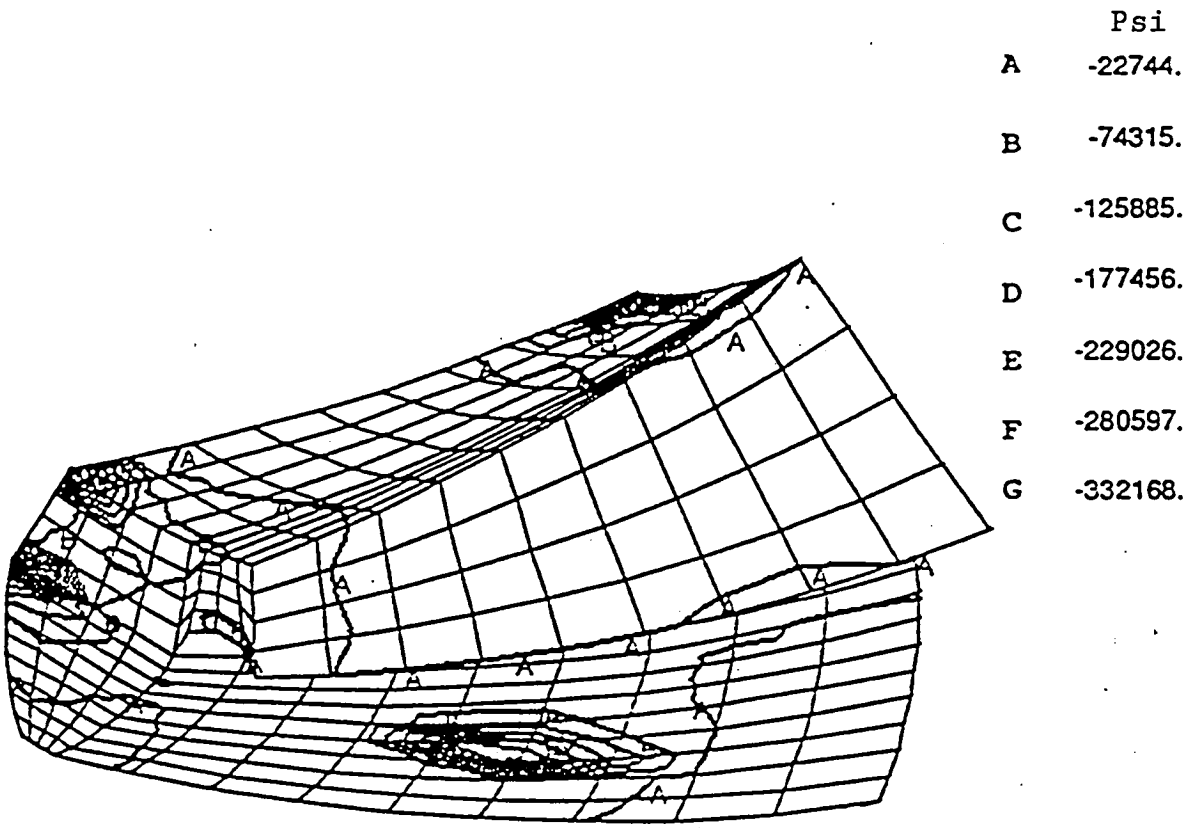


Figure 23. - Model II. Average nodal minimum principal stresses in pinion having major contact

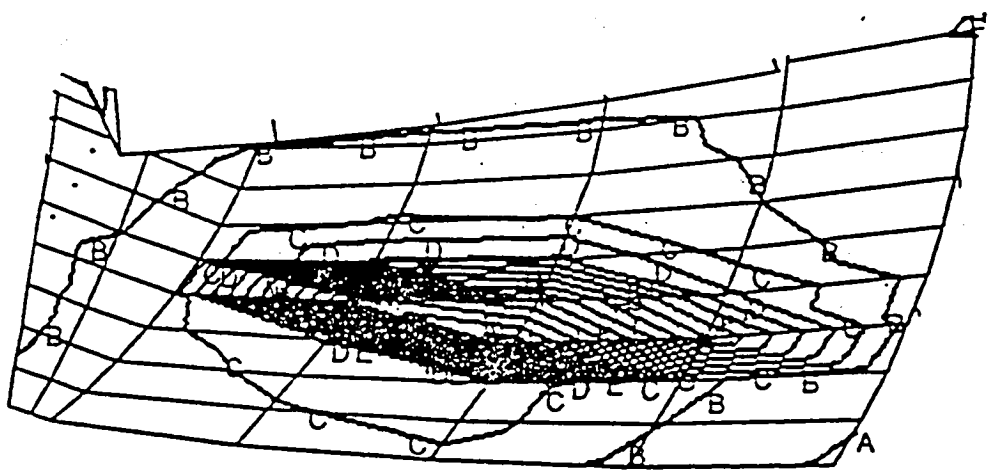

| | Psi |
|---|---|
| A | -8363. |
| B | -31170. |
| C | -53977. |
| D | -76784. |
| E | -99592. |
| F | -122399. |
| G | -145206. |
| H | -168013. |
| I | -190820. |
| J | -213628. |
| K | -236435. |
| L | -259242. |
| M | -282049. |
| N | -304856 |
| O | -327664 |

Figure 24. - Model II. Average nodal minimum principal stresses in pinion having edge contact.

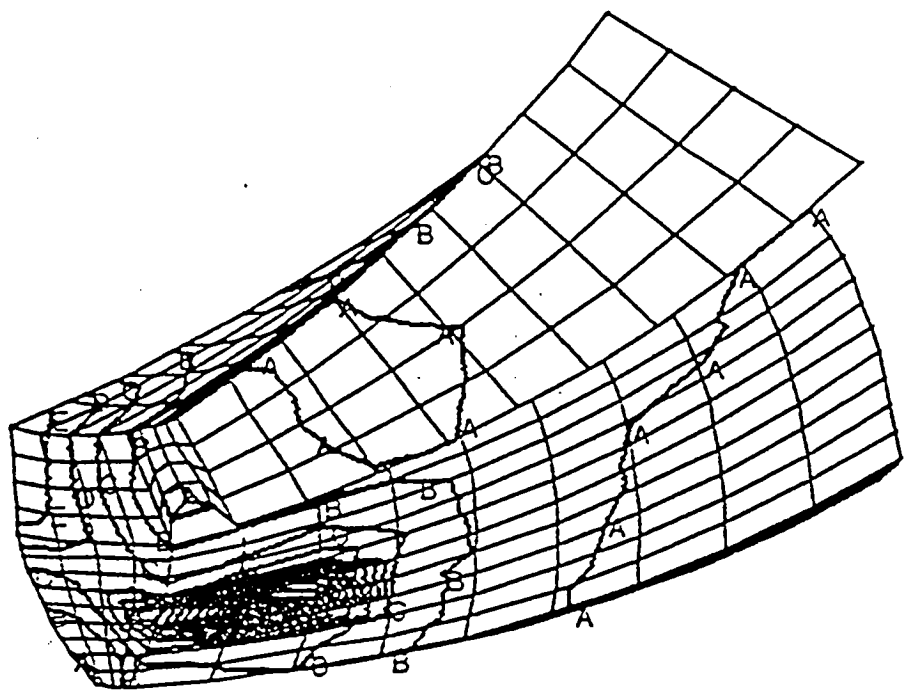

| | Psi |
|---|---|
| A | -1573. |
| B | -8476. |
| C | -15379. |
| D | -22281. |
| E | -29184. |
| F | -36087. |
| G | -42989. |
| H | -49892. |
| I | -56795. |
| J | -63698. |
| K | -70600. |
| L | -77503. |
| M | -84406. |
| N | -91308. |
| O | -98211. |

Figure 25. - Model II. Minimum principal element stresses in pinion having edge contact.

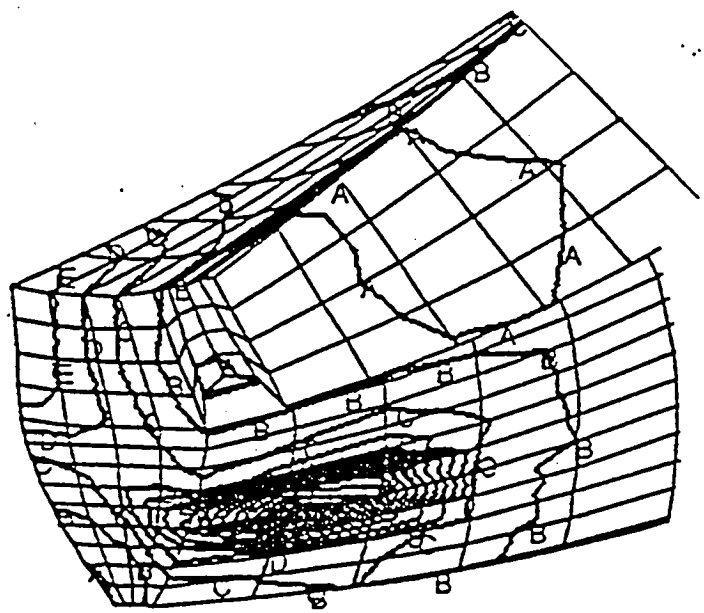

| | Psi |
|---|---|
| A | -1573. |
| B | -8476. |
| C | -15379. |
| D | -22281. |
| E | -29184. |
| F | -36087. |
| G | -42989. |
| H | -49892. |
| I | -56795. |
| J | -63698. |
| K | -70600. |
| L | -77503. |
| M | -84406. |
| N | -91308. |
| O | -98211. |

Figure 26.- Model II. Minimum principal element stresses at edge contact region in pinion.

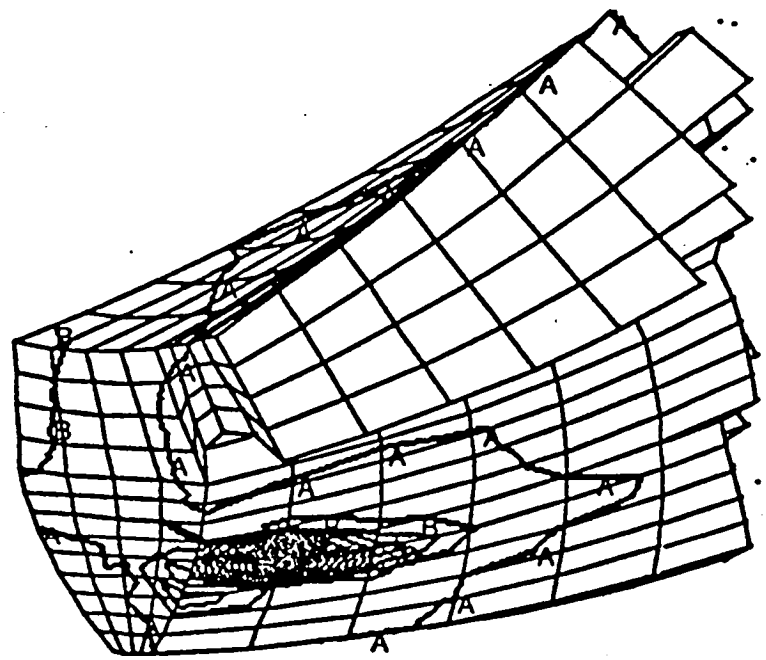

| | Psi |
|---|---|
| A | -12196. |
| B | -41355. |
| C | -70515. |
| D | -99674. |
| E | -128833. |
| F | -157993. |
| G | -187152. |
| H | -216311. |
| I | -245471. |
| J | -274630. |
| K | -303789. |
| L | -332949. |
| M | -362108. |
| N | -391267. |
| O | -420427. |

Figure 27. - Average nodal minimum prinicipal stresses in pinion having edge contact.

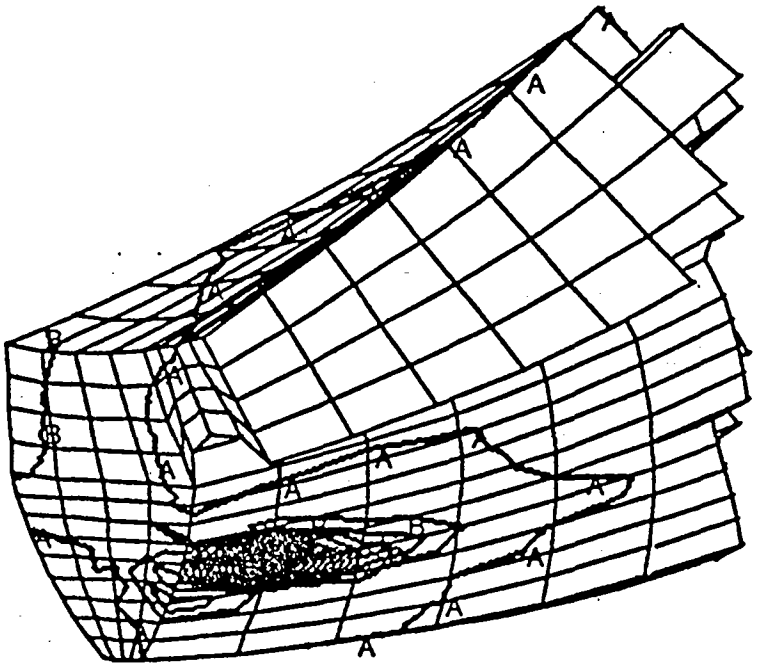

| | Psi |
|---|---|
| A | -12196. |
| B | -41355. |
| C | -70515. |
| D | -99674. |
| E | -128833. |
| F | -157993. |
| G | -187152. |
| H | -216311. |
| I | -245471. |
| J | -274630. |
| K | -303789. |
| L | -332949. |
| M | -362108. |
| N | -391267. |
| O | -420427. |

Figure 28. - Model II. Average nodal minimum principal stresses in pinion at edge contact region.

MAJOR CONTACT REGION GAP ELEMENTS

| | | | | |
|---|---|---|---|---|
| ⊙ | ⊙ | ⊙ | • | • |
| 1225 | 1228 | 1231 | 1234 | 1237 |
| • | • | ⊙ | ⊙ | • |
| 1226 | 1229 | 1232 | 1235 | 1238 |
| • | • | • | • | • |
| 1227 | 1230 | 1233 | 1236 | 1239 |

• GAP element number at the contact area
⊙ Closed GAP element number at the last iteration

EDGE CONTACT AREA GAP ELEMENT NUMBERS

| | |
|---|---|
| • | • |
| 6198 | 6201 |
| • | • |
| 6199 | 6202 |
| ⊙ | • |
| 6200 | 6203 |

GAP ELEMENTS CLOSED AFTER EACH ITERATION

| ITERATION 1 | ITERATION 2 | ITERATION 3 | ITERATION 4 |
|---|---|---|---|
| 1225 | 1225 | 1225 | 1225 |
| 1228 | 1228 | 1228 | 1228 |
| 1231 | 1231 | 1231 | 1231 |
| 1232 | 1232 | 1232 | 1232 |
| 1233 | 1233 | 1235 | 1235 |
| 1234 | 1235 | 6200 | 6200 |
| 1235 | 1239 | | |
| 1236 | 6200 | | |
| 1239 | | | |
| 6200 | | | |

FIGURE 29. Model II: GAP element status at each iteration.

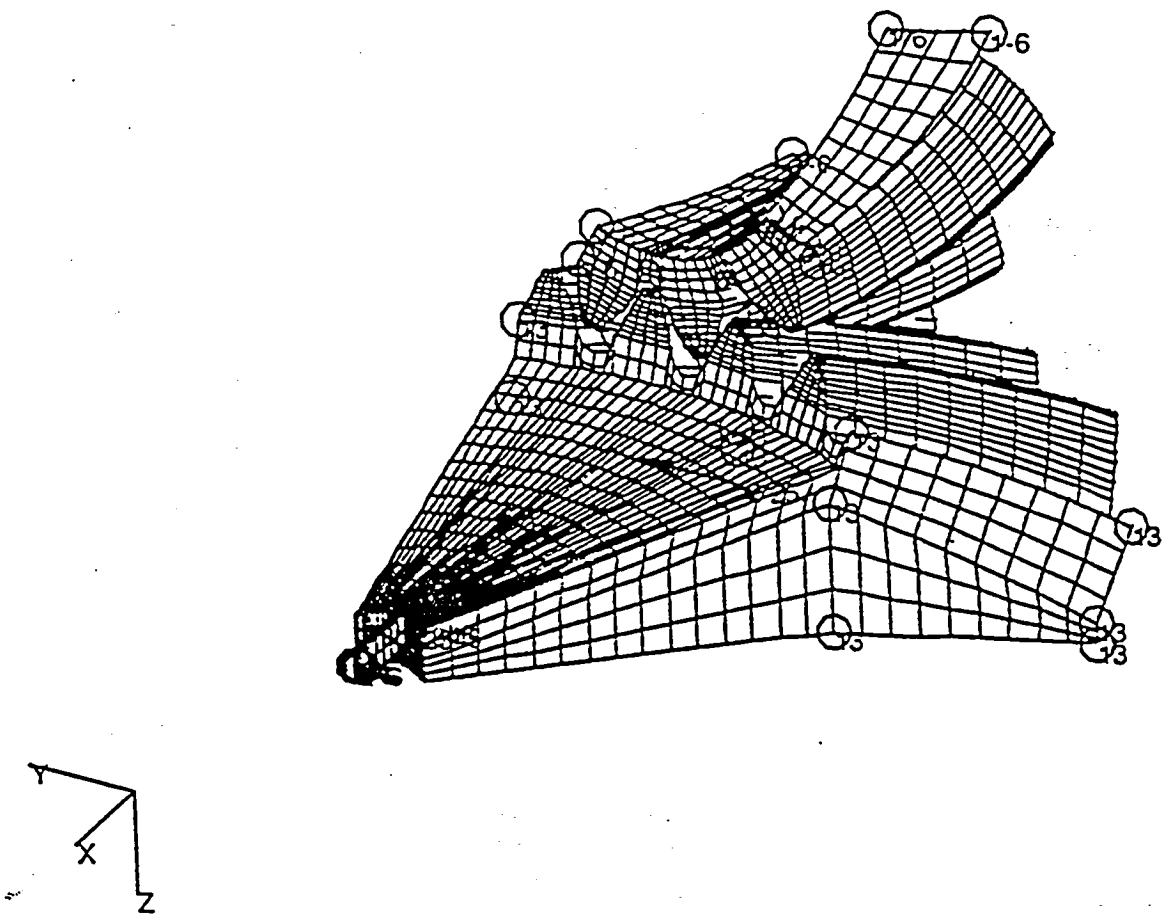


Figure 30. - Model III. Finite element model and boundary conditions

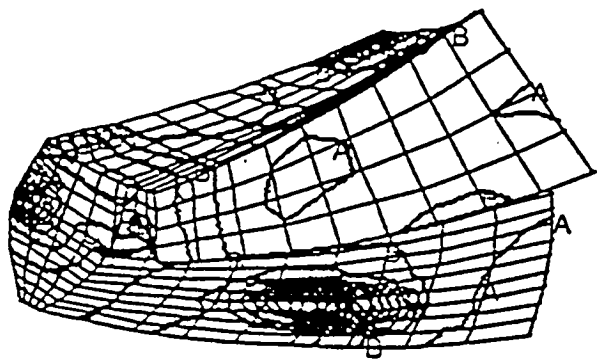

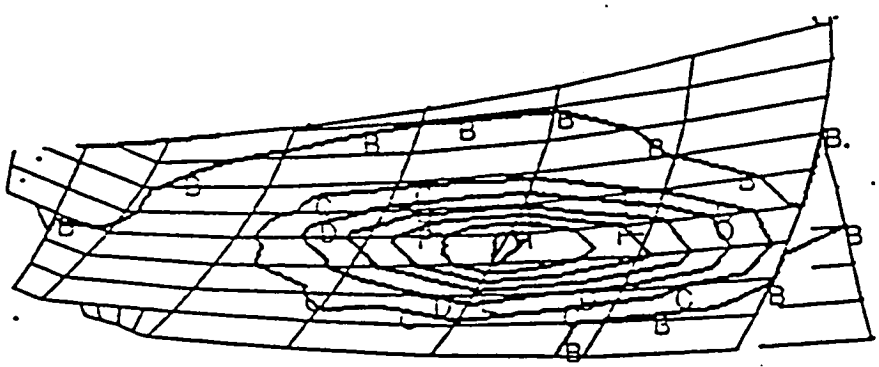

| | Psi |
|---|---|
| A | -5875 |
| B | -17145 |
| C | -28414 |
| D | -39683 |
| E | -50953 |
| F | -62222 |
| G | -73492 |
| H | -84761. |
| I | -96030. |
| J | -107300 |
| K | -118569 |
| L | -129838. |
| M | -141108. |
| N | -152377 |
| O | -163647 |

Figure 31. - Model III. Element minimum principal stresses in pinion at major contact region.

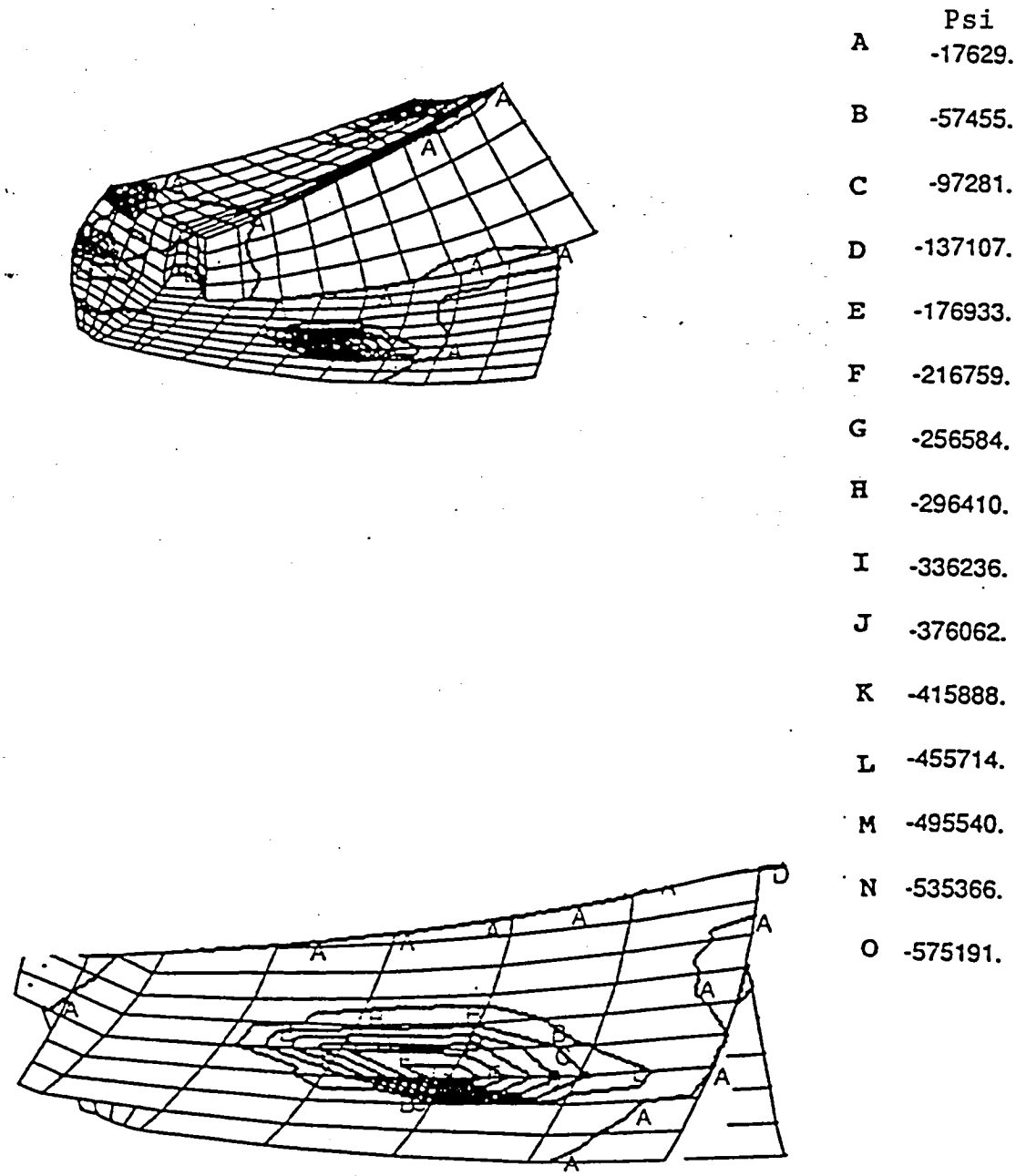


Figure 32. - Model III. Nodal minimum principal stresses in pinion at major contact region.

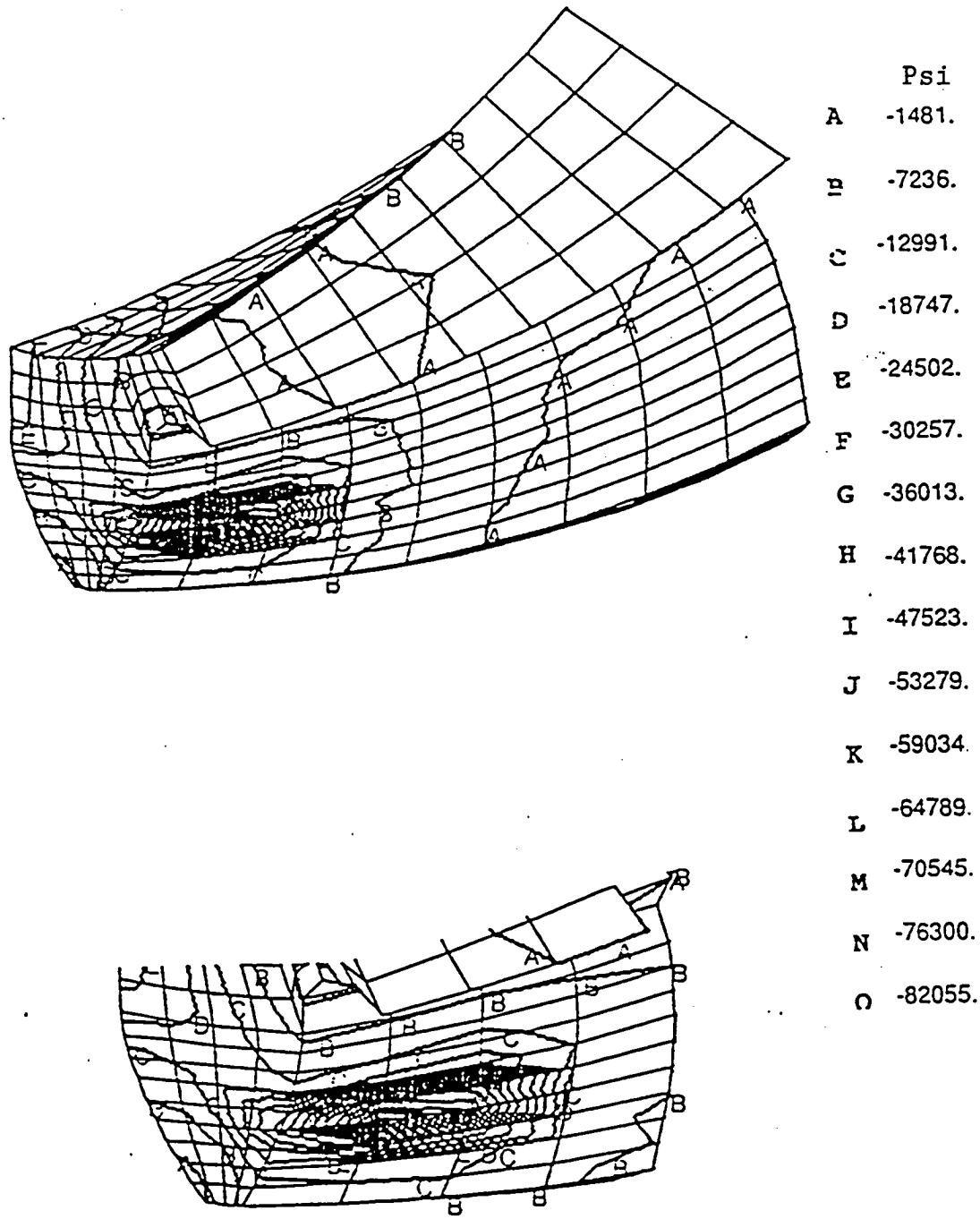


Figure 33. - Model III. Element principal stresses in pinion having edge contact

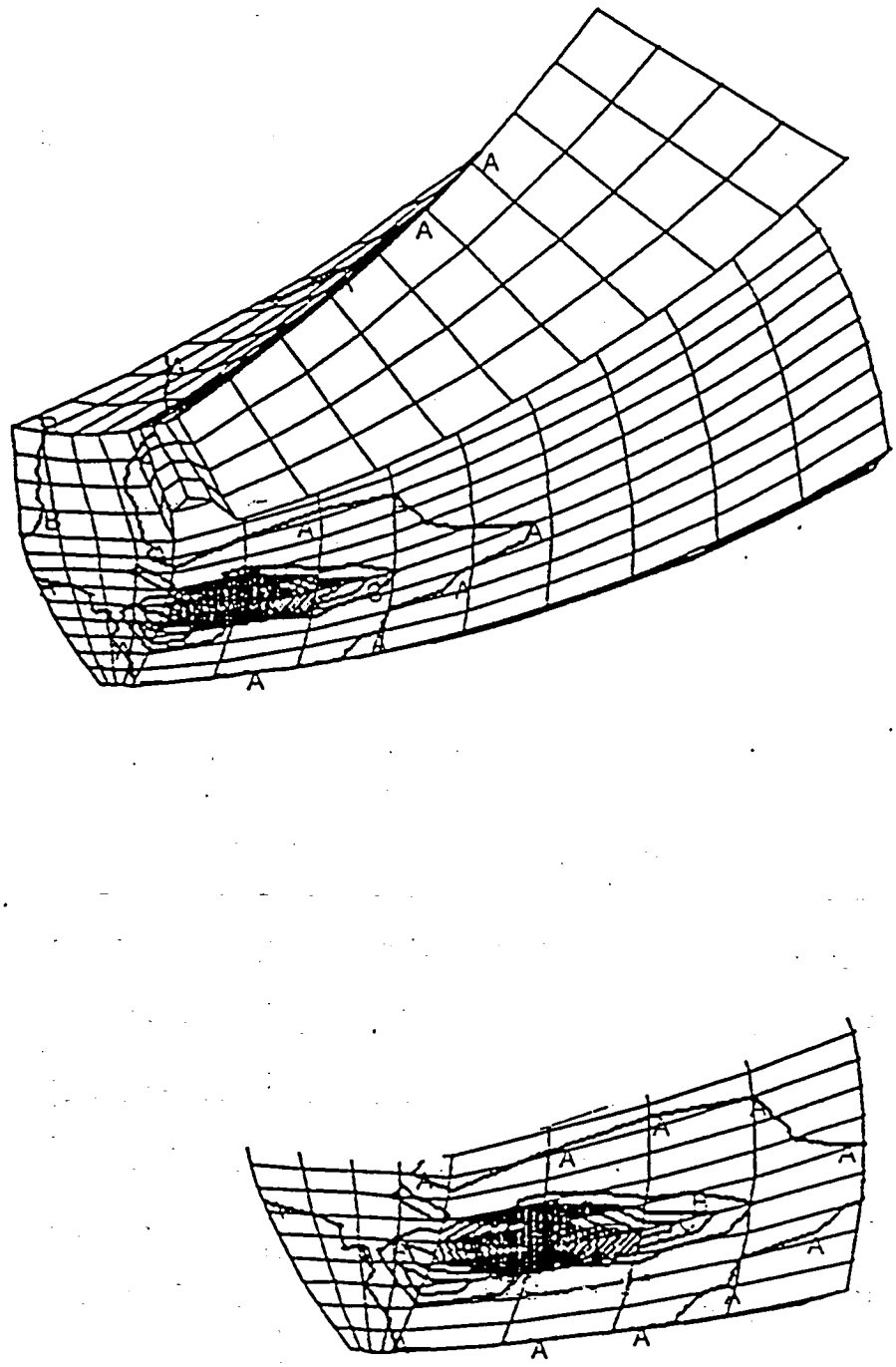

| | Psi |
|---|---|
| A | -10298. |
| B | -34672. |
| C | -59046. |
| D | -83420. |
| E | -107794. |
| F | -132169. |
| G | -156543. |
| H | -180917. |
| I | -205291. |
| J | -229665. |
| K | -254040. |
| L | -278414. |
| M | -302788. |
| N | -327162. |
| O | -351536. |

Figure 34. - Model III. Nodal principal stresses in pinion having edge contact

MAJOR CONTACT REGION GAP ELEMENTS

| | | | | |
|---|---|---|---|---|
| • 1225 | ⊙ 1228 | ⊙ 1231 | • 1234 | • 1237 |
| • 1226 | • 1229 | ⊙ 1232 | ⊙ 1235 | • 1238 |
| • 1227 | • 1230 | • 1233 | • 1236 | • 1239 |

• GAP element number at the contact area
⊙ Closed GAP element number at the last iteration

EDGE CONTACT AREA GAP ELEMENT NUMBERS

| | |
|---|---|
| • 6198 | • 6201 |
| • 6199 | • 6202 |
| ⊙ 6200 | • 6203 |

GAP ELEMENTS CLOSED AFTER EACH ITERATION

| ITERATION 1 | ITERATION 2 | ITERATION 3 | ITERATION 4 |
|---|---|---|---|
| 1228 | 1228 | 1228 | 1228 |
| 1229 | 1231 | 1231 | 1231 |
| 1231 | 1232 | 1232 | 1232 |
| 1232 | 1233 | 1235 | 1235 |
| 1233 | 1235 | 6200 | 6200 |
| 1235 | 6200 | | |
| 1236 | | | |
| 1239 | | | |
| 6200 | | | |

FIGURE 35.- Model III: GAP element status at each iteration.

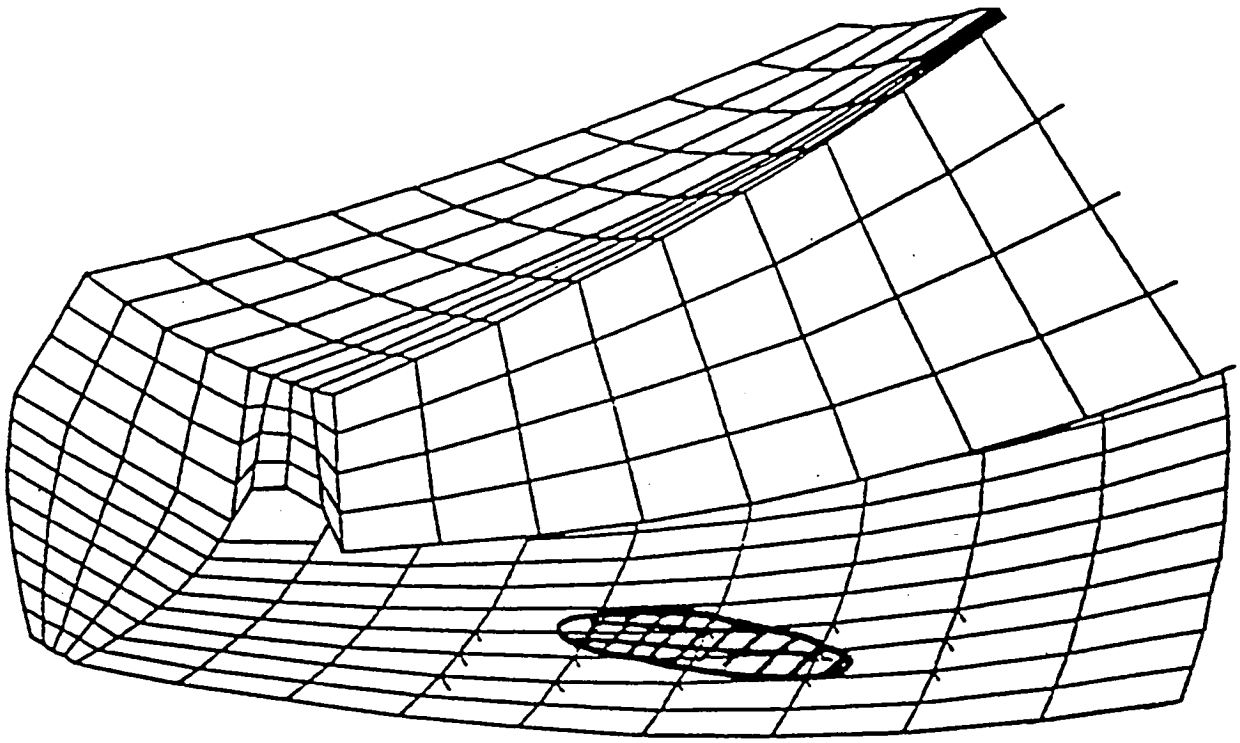

Figure 36. - Approximate contact region

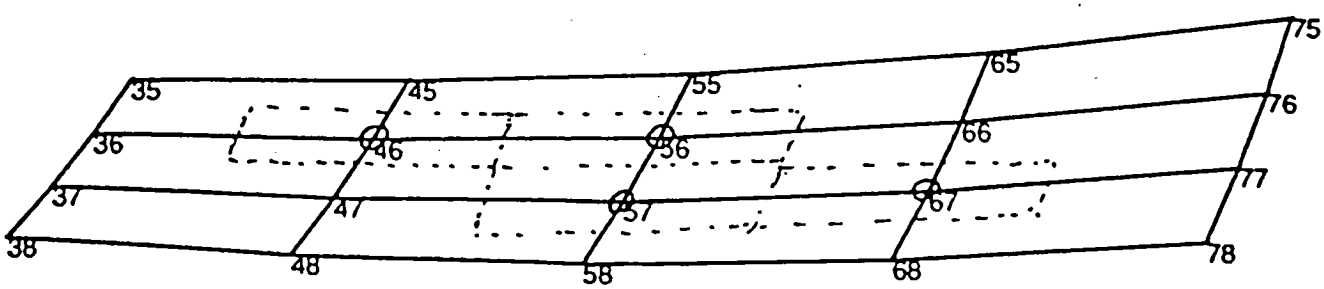


| | |
|---|---|
| DISTANCE BETWEEN GRIDS 56-46 | = 0.14302 in |
| DISTANCE BETWEEN GRIDS 46-47 | = 0.035118 in |
| APPROX. AREA OF EACH DASHED BOX | = 0.14032 * 0.035118 = 0.00492 sq.in |
| TOTAL AREA OF CONTACT | = 4 * 0.00492 = 0.01968 sq.in |

- GAP ELEMENTS CLOSED AFTER FINAL ITERATION
  AREA OF INFLUENCE OF GAP ELEMENTS

Figure 37 - Contact area calculation

TABLE I

MAJOR CONTACT AREA STRESSES

AVERAGE NODAL MINIMUM PRINCIPAL STRESSES (Psi)

| | | | | |
|---|---|---|---|---|
| -99,278 | -447,732 | -292,902 | -128,307 | -32,075 |
| -73,283 | -113,703 | -330,360 | -292,452 | -87,131 |
| -67,939 | -94,100 | -99,650 | -58,195 | -209,021 |

MINIMUM PRINCIPAL ELEMENT STRESS VALUES (Psi)

| | | | | |
|---|---|---|---|---|
| -76,077 | -155,833 | -195,923 | -120,920 | -35,158 |
| -65,956 | -113,892 | -181,131 | -151,829 | -61,995 |
| -58,335 | -76,757 | -98,768 | -85,134 | -59,703 |

Each box represents a grid point where the gap element is connected

TABLE II

MAJOR CONTACT AREA STRESSES

AVERAGE NODAL MINIMUM PRINCIPAL STRESSES (Psi)

| | | | | |
|---|---|---|---|---|
| -51,885 | -292,976 | -240,226 | -80,869 | -22,945 |
| -47,977 | -78,740 | -339,064 | -170,588 | -22,499 |
| -42,036 | -61,329 | -63,651 | -35,836 | -13,255 |

MINIMUM PRINCIPAL ELEMENT STRESS VALUES (Psi)

| | | | | |
|---|---|---|---|---|
| -42,615 | -104,243 | -156,041 | -97,885 | -21,234 |
| -38,595 | -77,441 | -148,742 | -120,439 | -29,393 |
| -37,185 | -51,781 | -77,700 | -62,839 | -20,692 |

EDGE CONTACT AREA STRESSES

AVERAGE NODAL MINIMUM PRINCIPAL STRESSES (PSI)

| | |
|---|---|
| -53,979 | -47,887 |
| -222,448 | -123,496 |
| -435,002 | -481,34 |

MINIMUM PRINCIPAL ELEMENT STRESSES (PSI)

| | |
|---|---|
| -25,826 | -67,699 |
| -74,485 | -83,260 |
| -101,661 | -42,817 |

Each box represents a grid point where the GAP element is connected

TABLE III

MAJOR CONTACT AREA STRESSES

AVERAGE NODAL MINIMUM PRINCIPAL STRESSES (Psi)

| | | | | |
|---|---|---|---|---|
| -39,532 | -213,109 | -200,745 | -51,752 | -17,504 |
| -39,085 | -64,462 | -299,931 | -103,574 | -16,417 |
| -32,710 | -49,034 | -50,525 | -28,640 | -9,714 |

MINIMUM PRINCIPAL ELEMENT STRESS VALUES (Psi)

| | | | | |
|---|---|---|---|---|
| -32,508 | -79,585 | -123,967 | -75,732 | -13,044 |
| -29,618 | -60,895 | -120,019 | -90,893 | -17,253 |
| -28,952 | -41,204 | -62,573 | -47,993 | -140,90 |

EDGE CONTACT AREA STRESSES

AVERAGE NODAL MINIMUM PRINCIPAL STRESSES (PSI)

| | |
|---|---|
| -45,042 | -39,566 |
| -185,999 | -102,755 |
| -363,720 | -39,929 |

MINIMUM PRINCIPAL ELEMENT STRESSES (PSI)

| | |
|---|---|
| -21,387 | -56,272 |
| -65,541 | -69,223 |
| -84,932 | -35,293 |

Each box represents a grid point where the gap element is connected

# REPORT DOCUMENTATION PAGE

Form Approved
OMB No. 0704-0188

Public reporting burden for this collection of information is estimated to average 1 hour per response, including the time for reviewing instructions, searching existing data sources, gathering and maintaining the data needed, and completing and reviewing the collection of information. Send comments regarding this burden estimate or any other aspect of this collection of information, including suggestions for reducing this burden, to Washington Headquarters Services, Directorate for Information Operations and Reports, 1215 Jefferson Davis Highway, Suite 1204, Arlington, VA 22202-4302, and to the Office of Management and Budget, Paperwork Reduction Project (0704-0188), Washington, DC 20503.

**1. AGENCY USE ONLY** (*Leave blank*)

**2. REPORT DATE**
March 1994

**3. REPORT TYPE AND DATES COVERED**
Final Contractor Report

**4. TITLE AND SUBTITLE**
A Procedure for 3-D Contact Stress Analysis of Spiral Bevel Gears

**5. FUNDING NUMBERS**
WU–505–62–10
C–NAG3–1476
1L162211A47A

**6. AUTHOR(S)**
A. Kumar and G. Bibel

**7. PERFORMING ORGANIZATION NAME(S) AND ADDRESS(ES)**
University of Akron
Akron, Ohio 44325

**8. PERFORMING ORGANIZATION REPORT NUMBER**
E–8613

**9. SPONSORING/MONITORING AGENCY NAME(S) AND ADDRESS(ES)**
Vehicle Propulsion Directorate
U.S. Army Research Laboratory
Cleveland, Ohio 44135–3191
and
NASA Lewis Research Center
Cleveland, Ohio 44135–3191

**10. SPONSORING/MONITORING AGENCY REPORT NUMBER**
NASA CR–194472
ARL–CR–72

**11. SUPPLEMENTARY NOTES**
A. Kumar, University of Akron; and G. Bibel, University of North Dakota, Grand Forks, North Dakota 58201. Project Manager, Robert F. Handschuh, Propulsion Systems Division, organization code 2730, NASA Lewis Research Center, (216) 433–3969.

**12a. DISTRIBUTION/AVAILABILITY STATEMENT**
Unclassified - Unlimited
Subject Category 37

**12b. DISTRIBUTION CODE**

**13. ABSTRACT** ***(Maximum 200 words)***

Contact stress distribution of spiral bevel gears using non-linear finite element static analysis is presented. Procedures have been developed to solve the non-linear equations that identify the gear and pinion surface coordinates based on the kinematics of the cutting process; and, orientate the pinion and the gear in space to mesh with each other. Contact is simulated by connecting GAP elements along the intersection of a line from each pinion point (parallel to the normal at the contact point) with the gear surface. A three-dimensional model with four gear teeth and three pinion teeth is used to determine the contact stresses at two different contact positions in a spiral bevel gearset. A summary of the elliptical contact stress distribution is given. This information will be helpful to helicopter and aircraft transmission designers who need to minimize weight of the transmission and maximize reliability.

**14. SUBJECT TERMS**
Gears; Gear teeth; Transmissions; Finite elements

**15. NUMBER OF PAGES**
79

**16. PRICE CODE**
A05

**17. SECURITY CLASSIFICATION OF REPORT**
Unclassified

**18. SECURITY CLASSIFICATION OF THIS PAGE**
Unclassified

**19. SECURITY CLASSIFICATION OF ABSTRACT**

**20. LIMITATION OF ABSTRACT**